SPEx enables compartment-resolved proteomics via expansion microscopy–guided microdissection

Curdin A Franziscus, Alexia Ferrand, Oliver Biehlmaier, Alexander Schmidt*, Anne Spang*

Biozentrum, University of Basel, Basel, Switzerland

eLife Assessment

Franziscus et al. present an **important** study introducing SPEx, an elegant, broadly accessible approach to subcellular spatial proteomics that combines cell expansion, laser microdissection, and mass spectrometry to enable protein profiling within defined subcellular regions. The authors provide **convincing** evidence that this flexible integration of established techniques offers a robust, practical, and cost-effective strategy for compartment-resolved proteomic analysis. The method is appropriately validated across multiple subcellular compartments and complementary workflows, demonstrating its ability to recover known protein markers while identifying previously uncharacterised components. The study also provides a characterisation of the method's capabilities and limitations. Overall, SPEx is likely to be of broad interest to cell biologists seeking to map organelle composition.

***For correspondence:** alex.schmidt@unibas.ch (AS); anne.spang@unibas.ch (AS)

Competing interest: The authors declare that no competing interests exist.

Funding: See page 21

Preprint posted 30 March 2026
Sent for Review 28 March 2026
Reviewed preprint v1 27 May 2026
Reviewed preprint v2 09 November 2026
Version of Record 26 November 2026

Reviewing Editor: Ishier Raote, Institut Jacques Monod, France

© Copyright Franziscus *et al.* This article is distributed under the terms of the Creative Commons Attribution License, which permits unrestricted use and redistribution provided that the original author and source are credited.

Abstract Cells contain different organelles and compartments that are essential for cellular function and life. These organelles and compartments need to communicate to assess cellular state in a changing environment, adapt to the new situation, and to ensure functionality and homeostasis. Moreover, organization and communication differ between cell types. However, our knowledge about these changes is still rather scarce. Subcellular spatial proteomics aims to fill this knowledge gap. While proximity labeling techniques represent a great advance, they do not provide precise spatial resolution. To overcome this limitation, we developed SPEx (*S*ubcellular spatial *P*roteomics coupled to *Ex*pansion), in which we first expand cells about tenfold, laser micro-dissect regions of interest, and then perform mass spectrometry-based proteomics on these samples. We demonstrate the effectiveness of SPEx by determining the proteome of the Golgi, the nucleus, and the nucleoli. Importantly, we also identify novel components of these organelles. Combining inexpensive, already existing technologies makes SPEx readily usable by the wider scientific community.

Introduction

Intracellular communication is essential for any life form. The communication, however, changes depending on a multitude of inputs such as extracellular cues, cell-cycle stage, nutrient availability, stress, and age. This adaptability is key to the survival of any organism. While our understanding is increasing about intracellular communication in a few model organisms, such as tissue culture cells, *Drosophila*, *Caenorhabditis elegans,* and yeast in unperturbed conditions, we still lack understanding how communication changes under different conditions and in different cell types. Efforts to fill this knowledge gap are hampered by the fact that the basic machinery is often the same, but with variations in the interactions and composition of complexes or specific temporal and spatial regulation.

Spatial subcellular proteomics intends to overcome this knowledge gap and aims to determine the localizations, concentrations, and interactions of proteins within cells and tissues, while preserving their spatial information (**Lundberg and Borner, 2019**). A number of techniques have been developed to perform spatial proteomics at a subcellular resolution including differential centrifugation, organellar immunoprecipitation, and proximity labeling methods (**Fasimoye et al., 2023**; **Geladaki et al., 2019**; **Hundley et al., 2024**; **Lundberg and Borner, 2019**; **Roux et al., 2012**). These techniques greatly improved our understanding of cellular organization and allowed the creation of comprehensive databases where large parts of, for example, the human proteome are mapped to specific subcellular compartments. However, all these approaches identify proteins based on proximity or co-purification with known markers and not on actual spatial positional information. This shortcoming cannot be circumvented since these techniques rely on a lysis step prior to proteomic analysis and hence all spatial information is inevitably lost.

More recently, Microscoop aimed to overcome these drawbacks by introducing a technique that allows laser-guided biotinylation of specific subcellular regions in situ, whose protein content can be determined by subsequent cell lysis, biotin pulldown, and liquid chromatography-mass spectrometry (LC-MS)-based proteomic analysis (**Chang et al., 2024**; **Chen et al., 2023**). While allowing for high spatial resolution, the laser-guided biotinylation of the region of interest (ROIs) is very time-consuming and expensive. The subsequent affinity purification step requires the labeling of a rather large number of ROIs and cells, contributing to the substantial costs and low throughput. Because of the large number of required ROIs, this technique critically depends on automatization through machine learning algorithms and highly specialized equipment that are not readily available in most universities and research institutes. While an interesting technology, these drawbacks might limit the accessibility of Microscoop for the wider scientific community.

Conversely, laser microdissection (LMD) allows direct LC-MS analysis of ROIs of tissues, cells, or subcellular regions and does not require a time- and sample-consuming affinity purification step. This method has been successfully applied to determine the proteome of single cells within tissues (**Herrera et al., 2020**; **Le Large et al., 2020**; **Rosenberger et al., 2025**; **Rosenberger et al., 2023**) and is already an established and available workflow in many proteomics laboratories. Despite its recent success, this method is limited by its laser beam diameter (0.5–1 µm), which only allows collection of samples ranging from 5 to 10 µm in diameter (**Domazet et al., 2008**; **Walavalkar et al., 2025**). The combination of expansion microscopy (ExM) and LC-MS has been applied in the past on tissues to isolate and analyze multi-cell regions within tissues with a diameter of ~160 µm or more (**Li et al., 2022**). Technical limitations largely prevented its application for subcellular spatial proteomics apart from isolation of nuclei from 4x expanded cells (**Dong et al., 2024**).

Here, we introduce SPEx (*S*ubcellular spatial *P*roteomics coupled to *Ex*pansion), a novel technique that extends the application of LMD and LC-MS analysis to single micron subcellular ROIs by combining 10x expansion of samples using a hydrogel with LMD. To allow for 10x expansion of cultured cells, SPEx utilizes the well-established TREx protocol developed for ExM (**Damstra et al., 2022**). This boost in expansion greatly increases the resolution of LMD and enables the dissection of individual organelles at a single micrometer resolution. Furthermore, we demonstrate that SPEx allows the determination of the proteome of a diverse group of organelles differing in size and shape. Moreover, we identified novel protein components of organelles. The quantitative aspect of our method provides also information on relative enrichment or depletion of proteins localizing to different parts/organelles in the cell. Strikingly, with the introduction of ultra-sensitive LC-MS platforms designed for single-cell analysis (**Brunner et al., 2022**; **Guzman et al., 2024**), reasonable proteome coverage can be obtained with as little as about two dozen organelles. Moreover, SPEx is highly versatile and circumvents the need to develop specific protocols for the isolation of distinct organelles or cellular regions. SPEx relies exclusively on the visual selection of ROIs by the experimenter, based on fluorescent antibodies and/or dyes. In summary, we present SPEx, a novel kit-free, inexpensive, low-input method for in situ spatial proteomics at a micrometer resolution.

Results

Development of the SPEx method

Expansion microscopy

To overcome the need for an accessible, inexpensive subcellular spatial proteomics method, we developed SPEx (***Figure 1A***). This method combines ExM, LMD, and LC-MS analysis. First, HeLa cells are fixed, and the cellular structure(s) of interest is/are labelled with antibodies as in standard immunofluorescence (IF). In the present study, we labelled the Golgi apparatus with an anti-GM130 antibody. To visualize the cell, we labelled all proteins non-specifically with fluorescent N-hydroxysuccinimide (NHS) ester (***Sheard et al., 2023***). For the efficient dissection of subcellular structures, we aimed for a robust expansion of about 10x, while preserving downstream compatibility to LC-MS proteomic analysis. A protein disruption step is necessary to suppress the non-covalent interactions in the cells. Typically, a protease treatment step (e.g. proteinase K), which is degrading proteins prior to expansion, is included to obtain high expansion factors (***Chen et al., 2015***; ***Tillberg et al., 2016***; ***Wen et al., 2023***). We cannot use protease treatment because it is incompatible with downstream LC-MS. Instead, we used sodium dodecyl sulfate (SDS) denaturation as described in the U-ExM or TREx protocols (***Damstra et al., 2022***; ***Gambarotto et al., 2019***). To confirm that this alternative was suitable for LC-MS analysis, we tested whether such expanded samples still contained intact peptides that could be efficiently extracted from the gel. Indeed, the SDS treatment and expansion were compatible with proteomics. Moreover, we found that the sample size could be relatively small, while still maintaining good proteome coverage (***Figure 2—figure supplement 1A*** and ***Supplementary file 1A and B***). While most of the ExM publications use protease treatment for disruption to reach the 10x expansion (***Chen et al., 2015***; ***Tillberg et al., 2016***; ***Wen et al., 2023***), SDS denaturation only gave us an expansion factor ranging from four- to sevenfold, while the gels themselves expanded 10x. Due to this variability, we decided to adjust the TREx protocol (***Damstra et al., 2022***) to ensure a robust and high expansion factor. After reducing the anchoring between the proteins and matrix and performing an overnight denaturation at 95 °C, we consistently obtained ~9x expansion without protease treatment. This expansion represents an about 100x increase in area. At this expansion level, the fluorescence intensity was strong enough to detect the Golgi as well as proteins labeled with the NHS ester (***Figure 1B and C***). Of note, the strongest staining with the NHS ester was observed in the nucleus, and, in particular, in the nucleoli. Because the nuclei were strongly labeled by the NHS ester, we used the difference of the average nuclear diameter across a number of randomly selected cells before and after expansion as a surrogate for expansion factor determination (***Liffner et al., 2024***; ***Figure 1D and E***).

Laser microdissection

The aqueous properties of the gels were incompatible with laser cutting, due to laser diffraction and strong surface tension. To be able to collect organelles by LMD, we completely dried the expanded gels on the polyphenylene sulfide (PPS) membrane slides. This procedure conserved the fluorescence signal from both, NHS dyes as well as secondary antibodies, which is used for LMD (***Figure 2A and B***). Conveniently, the drying of the gels did not lead to severe shrinkage in length and width (x–y direction), but only in height (z-direction; ***Figure 2C,D***, ***Figure 2—figure supplement 1B***). Thus, we routinely retained an expansion of about 7x in x–y direction. The dried gels allowed efficient cutting at subcellular resolution using a Leica LMD7 system (***Figure 2E***, ***Figure 2—video 1***). We concentrated our efforts on three different organelles: the nucleus, the membraneless nucleolus, which were both nicely stained with the NHS ester, and the Golgi apparatus, visualized by anti-GM130. A summary of the number of cells and organelles, and which objective magnification was used to cut cells and organelles are outlined in ***Supplementary file 1C***. We did not only isolate these organelles from individual cells but also excised the exact same cells from which the nucleus/Golgi apparatus were removed (CellsMinusNucleus/CellsMinusGolgi; ***Figure 2E***). Similarly, after sampling the nucleoli, we also cut the nuclei from which the nucleoli were taken (NucleiMinusNucleoli; ***Figure 2E***). This was only possible because laser dissection allowed for repeated sampling from the same cell, without compromising sample quality.

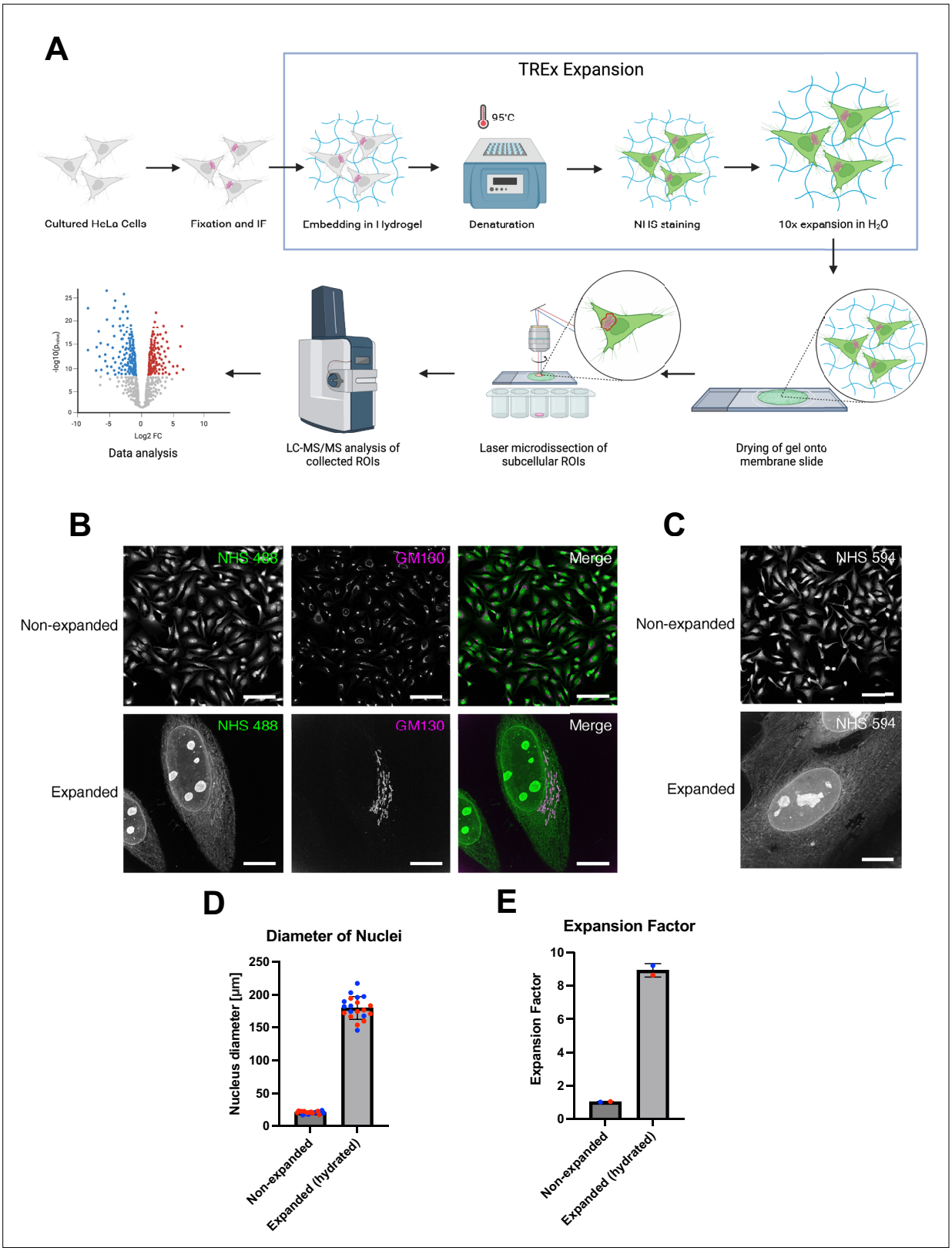


Figure 1. Development of the SPEx (*S*ubcellular spatial *P*roteomics coupled to *Ex*pansion) protocol. (**A**) SPEx workflow. Cultured HeLa cells are fixed, and immunofluorescence is used to label the subcellular compartment of interest with fluorescent antibodies. Next, the cells are embedded in a hydrogel. To allow for later expansion, proteins are denatured overnight at 95 °C. N-hydroxysuccinimide (NHS) staining is performed to non-specifically label proteins before expansion of the gel in H_2O. Expanded gels are dried onto polyphenylene sulfide (PPS) membrane slides, and laser

Figure 1 continued on next page

Figure 1 continued

microdissection of the areas of interest is performed. LC-MS of the collected areas and subsequent data analysis are used to identify proteins enriched in specific subcellular compartments. Created with BioRender.com. (**B**) Cells stained for total protein content with NHS 488 and immunostained with a GM130 antibody, with and without expansion using a modified TREx protocol. Scale bar: 100 µm. (**C**) Cells stained for total protein content with NHS 594, with and without expansion using a modified TREx protocol. Scale bar: 100 µm. (**D**) Measured nuclear diameters for non-expanded and expanded (hydrated) cells. Data are plotted as mean ± SD (non-expanded: 20.53±1.94 µm; expanded [hydrated]: 179.70±17.26 µm; n=10 cells; N=2 independent experiments indicated by different colors). (**E**) Average expansion factor calculated based on the measurements in (**D**). Data are plotted as mean ± SD (expanded [hydrated]: 8.934±0.40; N=2 independent experiments indicated by different colors).

LC-MS analysis

The collected samples were then prepared for proteomics, using an optimized protocol for low-input samples based on previous spatial proteomics workflows and latest generation of highly sensitive time-of-flight (ToF) LC-MS instrumentation using DIA-PASEF data acquisition (***Makhmut et al., 2026***; ***Rosenberger et al., 2025***). Notably, we detected no artificial chemical lysine modifications from NHS-labeling or anchoring. In addition, we also analyzed the ratio of C-terminal lysine vs arginine peptides and did not detect any bias (***Figure 2—figure supplement 1C***). This indicates that, if existent, such modifications are sparse with negligible proteome coverage impact. We consistently detected between 1200 and 2800 proteins per sample (***Figure 2F*** and ***Supplementary file 1D and E***). As expected, the number of identified proteins correlated with organelle size, where whole cells had the highest and nucleoli the lowest number of proteins. Moreover, principal component analysis (PCA) revealed very good clustering of biological replicates and, with the exception of whole cell controls, distinct segregation of the different sample types (***Figure 2G***). Of note, the whole cell samples from the nuclei and Golgi experiments cluster nicely together, confirming robust proteome quantification of our SPEx workflow. Taken together, SPEx allows the expansion of cells, laser dissection of membrane-bounded and membraneless organelles, and detection of protein constituents in these organelles.

SPEx is suitable for the identification of nuclear proteins

To test the specificity and sensitivity of the SPEx method, we first applied it to the analysis of nuclear proteins from HeLa cells. The NHS ester allows the visualization of the entire cell and nucleus, and, hence, we cut out 25 nuclei from expanded cells and subjected them to LC-MS analysis. In addition, we analyzed the proteome of either 10 cells or 12 cells from which the nuclei had been dissected (CellsMinusNuclei). These samples were subjected to LC-MS analysis. First, we determined the percentage of the protein mass in the nuclei sample, which is contributed by proteins annotated to be located in the nucleus according to GO. We found that 75.5% of the total protein mass is contributed by nuclear proteins, indicating good purity (***Figure 3A***). Next, we compared either whole cells or CellsMinusNuclei to the nuclei sample. As expected, we observed much stronger abundance differences, and therefore a higher number of significantly enriched nuclear proteins, when comparing nuclei to CellsMinusNuclei rather than to WholeCells (***Figure 3B***, ***Figure 3—figure supplement 1A***). Moreover, the comparison of the proteome of the nuclei to the one of the remaining cells without nucleus minimizes cellular proteome variability. Using this comparison, we quantified around 2,200 proteins from only 25 nuclei (***Figure 2F*** and ***Supplementary file 1E***), with 522 proteins being significantly enriched in the nuclear samples. To evaluate the specificity of our approach, we checked the proportion of nuclear annotated proteins according to Gene Ontology (GO; ***Supplementary file 1F***) in the enriched protein fraction. We found 499 of the 522 proteins to be annotated nuclear, corresponding to a very high specificity of more than 95% (***Figure 3C***). Importantly, SPEx identified 23 proteins with strong nuclear enrichment that had not been annotated to be nuclear previously. Those proteins included SPOUT1 and C7orf50. Using IF on non-expanded HeLa cells, we confirmed the nuclear localization of C7orf50 (***Figure 3D***) and SPOUT1 (***Figure 4F***), validating the high spatial specificity achieved with our approach. In line with our findings, recently C7orf50 has been identified as an oncogene with an N-terminal nuclear localization signal (***Sun et al., 2026***). Mechanistically, it has been proposed to shuttle between the nucleoplasm and the nucleolus, regulating autophagy and ribosome biogenesis downstream of mTOR (***Sun et al., 2026***). As an additional specificity test, we performed a functional enrichment analysis, which confirmed all top significantly enriched categories to be nuclear (***Figure 3E*** and ***Supplementary file 1G***).

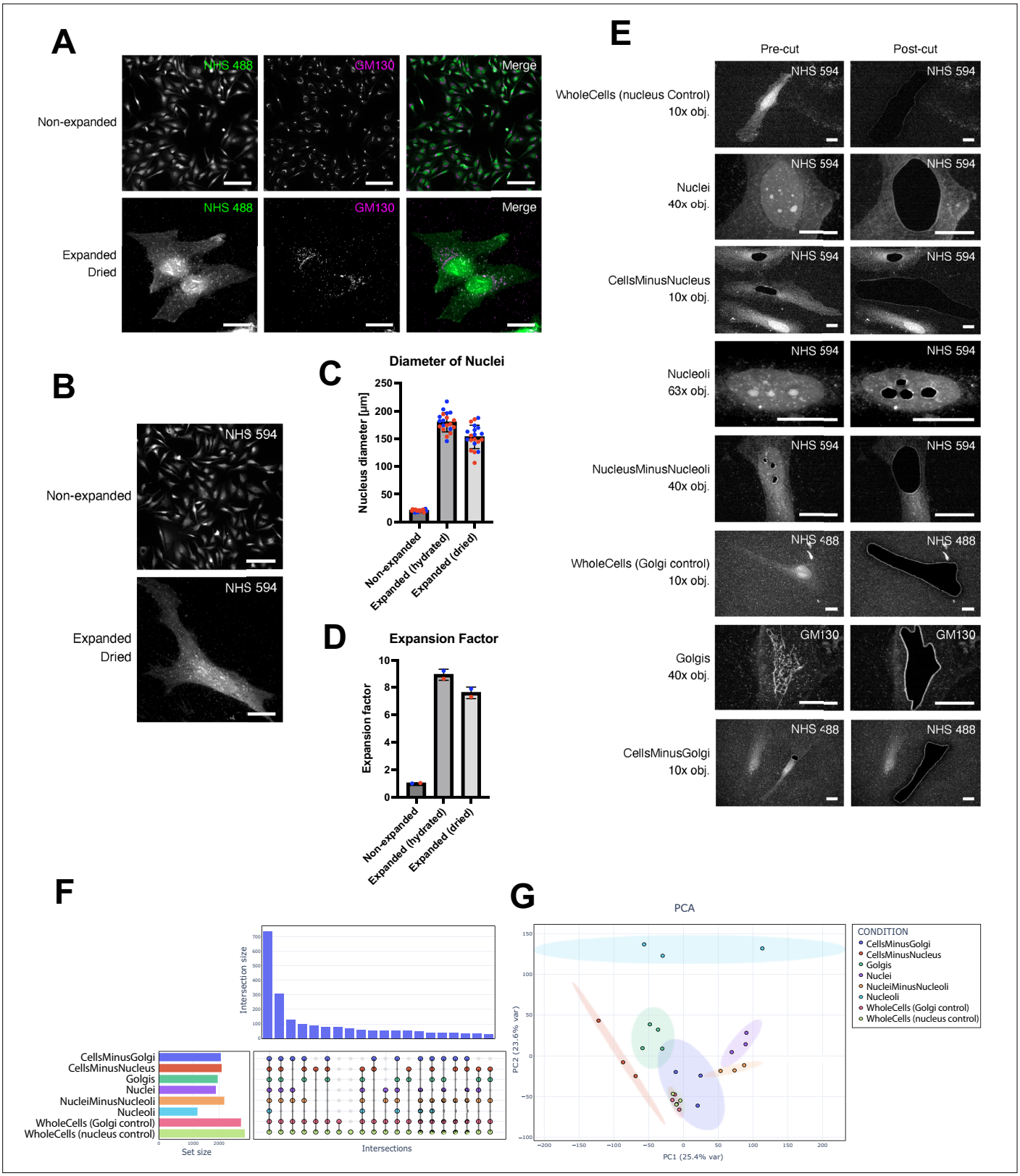


Figure 2. Optimization of the SPEx (*S*ubcellular spatial *P*roteomics coupled to *Ex*pansion) protocol for laser microdissection. (**A**) Cells stained for total protein with NHS 488 and immunostained for GM130, with and without expansion using a modified TREx protocol. Expanded samples were dried onto polyphenylene sulfide (PPS) membrane slides prior to imaging. Scale bar, 100 µm. (**B**) Cells stained for total protein with NHS 594, with and without expansion using a modified TREx protocol. Expanded samples were dried onto PPS membrane slides prior to imaging. Scale bar, 100 µm.

Figure 2 continued on next page

Figure 2 continued

(**C**) Nuclear diameters in non-expanded, expanded (hydrated and expanded (dried) cells). Data are mean ± SD (non-expanded: 20.53±1.94 µm; expanded (hydrated): 179.70±17.26 µm; expanded (dried): 153.30±21.16 µm; n=10 cells, N=2 independent experiments indicated by different colors). (**D**) Expansion factor calculated from measurements in (**C**). Data are mean ± SD (expanded (hydrated): 8.934±0.40; expanded (dried): 7.61±0.42; N=2 independent experiments indicated by different colors). (**E**) Pre- and post-cut images of all isolated sample types. Dissected cells were stained, expanded, and dried according to the SPEx protocol. Images are not to scale (magnification of the objective used for dissection is indicated). Scale bar, 100 µm. (**F**) UpSet plot showing shared and unique proteins identified across the different regions of interest (ROIs) shown in (**E**). The horizontal bar chart on the left (Set Size) indicates the total number of proteins identified in each compartment. The vertical bar chart on the top (intersection size) displays the number of proteins specific to each unique intersection or combination of sets, represented by the matrix of black dots and connecting lines in the lower panel. Single filled dots represent set-specific (exclusive) proteins, while vertically aligned connected dots represent overlapping intersections between multiple groups. The degree of intersection size is sorted by frequency. Total number of analyzed proteins across all sets is N=3021 (n=3 or 4 biological replicates per group). (**G**) Principal component analysis (PCA) of proteomics samples from the same ROIs shown in (**E**). The scatter plot shows the first two principal components, PC1 and PC2, which account for 25.4 and 23.6% of the total variance, respectively. Each data point represents an individual biological sample (n=3 or 4 per group). Colors and shapes indicate the distinct cell compartment groups. Ellipses represent the 95% confidence intervals for each group cluster.

The online version of this article includes the following video and figure supplement(s) for figure 2:

Figure supplement 1. Further optimization and quality control of the SPEx method.

Figure 2—video 1. Example movies of laser microdissection for all samples shown in ***Figure 2E***.
https://elifesciences.org/articles/111393/figures#fig2video1

Identification of proteins that are absent from the nucleus

Interestingly, functional enrichment analysis also identified significantly depleted cellular compartments, such as the plasma membrane and mitochondria (***Figure 3F***). Since cells without nuclei were used as a control for our analysis, SPEx can apparently not only be employed to localize proteins that are enriched in the nucleus but also detect those that are specifically depleted and hence absent from the nuclear fraction. This effect is already evident in the volcano plot, as proteins that are exclusively present in the cytoplasm (DHX57), peripherally associated with non-nuclear organelles (Golgi: LRBA and FAM3C) or constituents of those organelles (mitochondria: TIMM8A) are among the most significantly depleted proteins (***Figure 3B***).

Many proteins annotated to be nuclear by GO have either also functions in the cytoplasm and/or partition between the nucleus and other cellular locations. The quantitative capabilities of SPEx allowed us to define the primary location of a protein. Even if a protein is annotated to be nuclear by GO, but depleted in the nuclei sample, this protein is most likely in higher amount outside than inside the nucleus. For example, CLIP1 is annotated to be nuclear using GO. However, in our analysis, CLIP1 was strongly depleted from the nuclei (***Figure 3B***). In agreement with our findings, CLIP1 (CLIP-170) is a microtubule binding protein in the cytoplasm (***Perez et al., 1999***), also annotated as such in Uniprot, ProteinAtlas, and OpenCell (***Cho et al., 2022***; ***Nirschl et al., 2016***; ***The Human Protein Atlas, 2026***; ***Bateman et al., 2025***; ***Thul et al., 2017***). Likewise, SNTB2 was annotated to be nuclear by GO. In contrast, it is annotated to be in the cytoplasm according to UniProt and has a confirmed localization in the cytoplasm/Golgi in the Human Protein Atlas. Moreover, SNTB2 has been localized to the cytoplasm in adipocytes (***Krautbauer et al., 2019***). Thus, we confidently detect proteins that are strongly depleted from the nucleus. To take this analysis a step further, we wanted to assess the specificity of detection of non-nuclear proteins in the depleted fraction. Therefore, we determined the proportion of proteins annotated to be mitochondrial and absent from the list of nuclear annotated proteins. Overall, 164 proteins annotated 'mitochondrial' were found in our dataset and all but one of them were reduced in abundance in our nuclear sample (***Figure 3—figure supplement 1B***). Only SPOUT1 was found to be significantly enriched in the nuclear fraction, but this protein is wrongly annotated as it is actually not a mitochondrial protein but instead present in the nucleus (***Figure 4F***). Taken together, SPEx cannot only be used to quantitatively identify proteins specifically enriched in an organelle, but also proteins, whose concentrations are reduced in an organelle. The quantitative aspect of our approach makes it highly suitable for the analysis of changes in protein localization under different conditions.

Determining the nuclear proteome via a subtraction approach

Encouraged by these results and as another test of the quantitative aspect of our method, we asked whether we could determine the proteome by subtraction (***Figure 3—figure supplement 1C***).

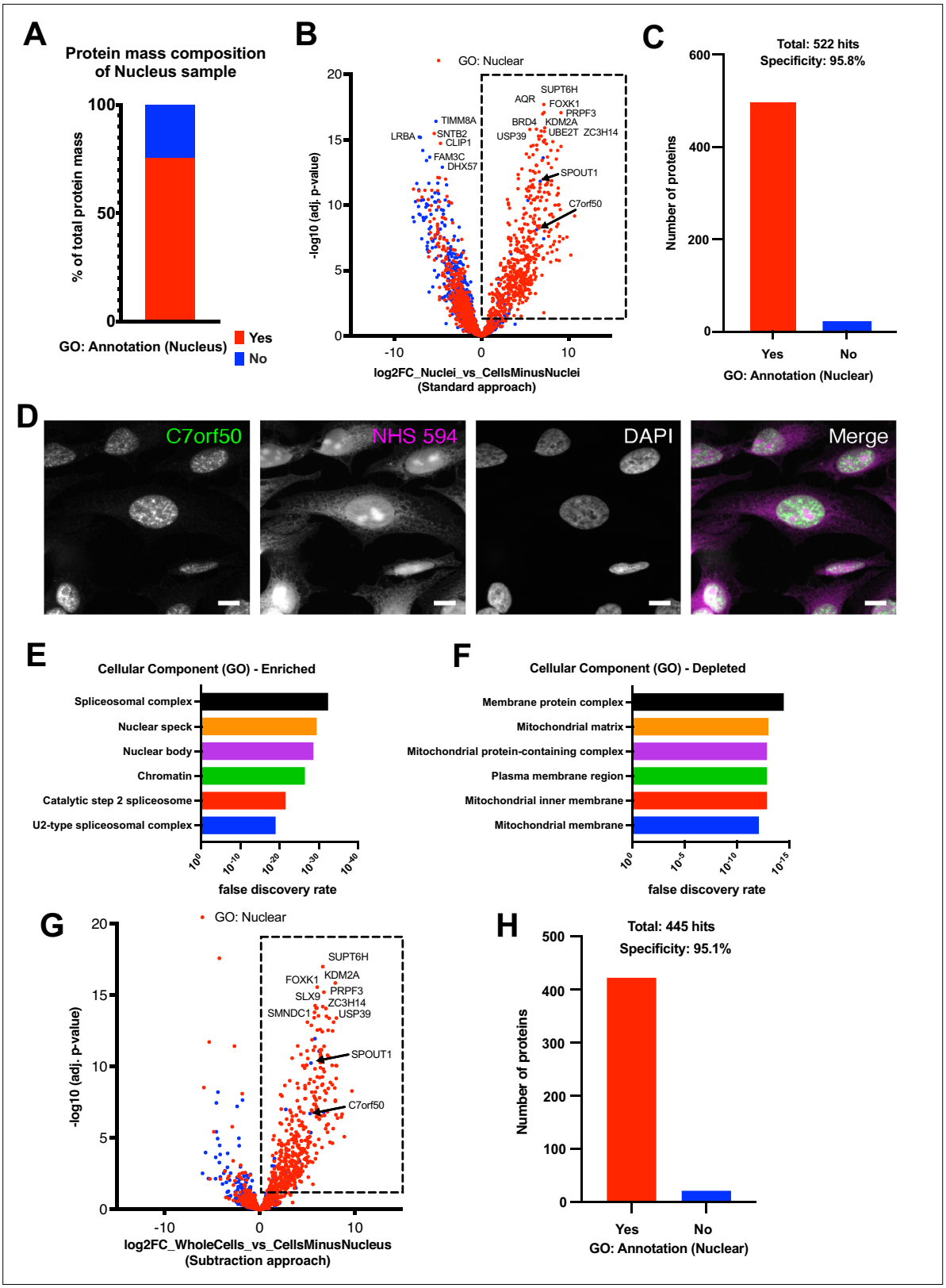


Figure 3. Application of SPEx (*Subcellular spatial Proteomics coupled to Expansion*) to the nucleus. (**A**) Protein mass composition of nucleus samples. Red bar indicates the percentage of protein mass contributed by proteins annotated as nuclear according to Gene Ontology (GO) to the total protein mass based on intensity-Based Absolute Quantification (iBAQ) values. (**B**) Volcano plot of pairwise proteomic comparison between nuclei and CellsMinusNuclei samples. The dotted square indicates proteins significantly enriched in the nucleus (adjusted $p<0.05$, $log_2FC >0$). Red dots represent

Figure 3 continued on next page

Figure 3 continued

proteins annotated as nuclear according to GO. FC, fold change. (**C**) Number of proteins significantly enriched in the nucleus in (B, dotted square) that are annotated as nuclear (Yes) or not nuclear (No) according to GO. (**D**) HeLa cells immunostained for C7orf50 and stained with 4′,6-Diamidin-2-phenylindol (DAPI) and NHS 594. DAPI is omitted from the merged image for clarity. Scale bar, 10 µm. (**E**) Functional enrichment analysis of all proteins shown in (**B**) for cellular components using GO via STRING (https://string-db.org/). The six most significantly enriched terms (ranked by FDR) are shown. All significant terms (FDR <1%) are listed in ***Supplementary file 1G***. (**F**) Same analysis as in (**E**), showing the six most significantly depleted GO terms. (**G**) Volcano plot of pairwise proteomic comparison between WholeCells and CellsMinusNucleus samples. The dotted square indicates proteins significantly enriched in WholeCells (adjusted $p<0.05$, $\log_2 FC >0$). Red dots represent proteins annotated as nuclear according to GO. (**H**) Same analysis as in (**C**) for proteins significantly enriched in WholeCells (G, dotted square).

The online version of this article includes the following figure supplement(s) for figure 3:

Figure supplement 1. Additional controls and comparisons to other methods for the application of SPEx to the nucleus.

Specifically, we wondered, if we compare the proteome of entire cells (WholeCells) to the one of cells from which we cut out the nucleus (CellsMinusNucleus), would we still be able to retrieve the nuclear proteome? We thought this might be feasible because the samples were well-separated in the PCA (***Figure 2G***). To our delight, this approach likewise showed a high enrichment of nuclear proteins (***Figure 3G and H***), achieving almost the same high specificity (95%) and coverage (423 nuclear proteins) compared to using the standard approach on the nuclei samples (***Figure 3B and C***). Moreover, the high overlap of the significantly enriched proteins confirmed the high specificity achieved with either comparison. In fact, about 400 proteins, which were common between the two analyses (***Figure 3—figure supplement 1D***) showed an extraordinary nuclear specificity of 98% (***Figure 3—figure supplement 1E***). Thus, the subtraction method can also be used to reliably identify the proteome of a compartment, without analyzing the compartment itself. Moreover, combining the two quantitative analyses can be used to further boost the specificity of the SPEx method.

SPEx compared to other spatial proteomics methods applied to the nucleus

To further assess the specificity and performance of our method, we next compared it to previously published large subcellular datasets, based on either subcellular fractionation followed by proteome profiling (***Geladaki et al., 2019***; ***Orre et al., 2019***) or native immunoprecipitation proteomics of organelles (***Hein et al., 2025***; ***Supplementary file 1HI and J***). While the other methods could overall identify more proteins in their nuclear fractions (***Figure 3—figure supplement 1F***), SPEx achieved the highest specificity of all datasets (***Figure 3—figure supplement 1G***).

Taken together, SPEx is a new method to identify reliably and with high specificity nuclear proteins from low input samples. SPEx serves also as a discovery tool as we identified unannotated nuclear proteins. Moreover, our method is quantitative and efficiently determined proteins that were depleted or absent from nuclei.

SPEx identifies the nucleolar proteome

To test whether SPEx also allows the determination of the proteome of much smaller structures within the cell, we aimed to investigate the proteome of nucleoli. Targeting nucleoli bears another challenge in that nucleoli are membraneless organelles, and many components are constantly exchanging between the nucleoplasm and the nucleoli, unlike when targeting a membrane-bounded organelle. Furthermore, the biochemical purification of membraneless organelles is challenging, and hence, the composition of the nucleolus is mostly based on imaging data or on GO annotation trained algorithm (***Hein et al., 2025***).

First, we aimed to confirm that the NHS ester-stained structures in the nucleus are indeed nucleoli. Therefore, we stained cells for nucleolin (NCL), an established nucleolar marker, or SON, which marks nuclear speckles (***Hondele et al., 2019***; ***Su et al., 2013***). Indeed, NHS ester marks specifically nucleoli and not nuclear speckles (***Figure 4A***). We therefore cut out 100 nucleoli and subsequently the corresponding nuclei without nucleoli (NucleiMinusNucleoli) and compared their proteomes (***Figure 4—figure supplement 1A***). We detect about 300 proteins, of which according to GO only 11% were annotated to be nucleolar localized (***Figure 4—figure supplement 1B***). This was also reflected in the mass contribution of proteins which are annotated as nucleolar according to GO, which was only 3.9% (***Figure 4—figure supplement 1C***). One reason could be that most nucleolar proteins shuttle between the nucleoli and the nucleoplasm, and therefore their abundance could be rather similar

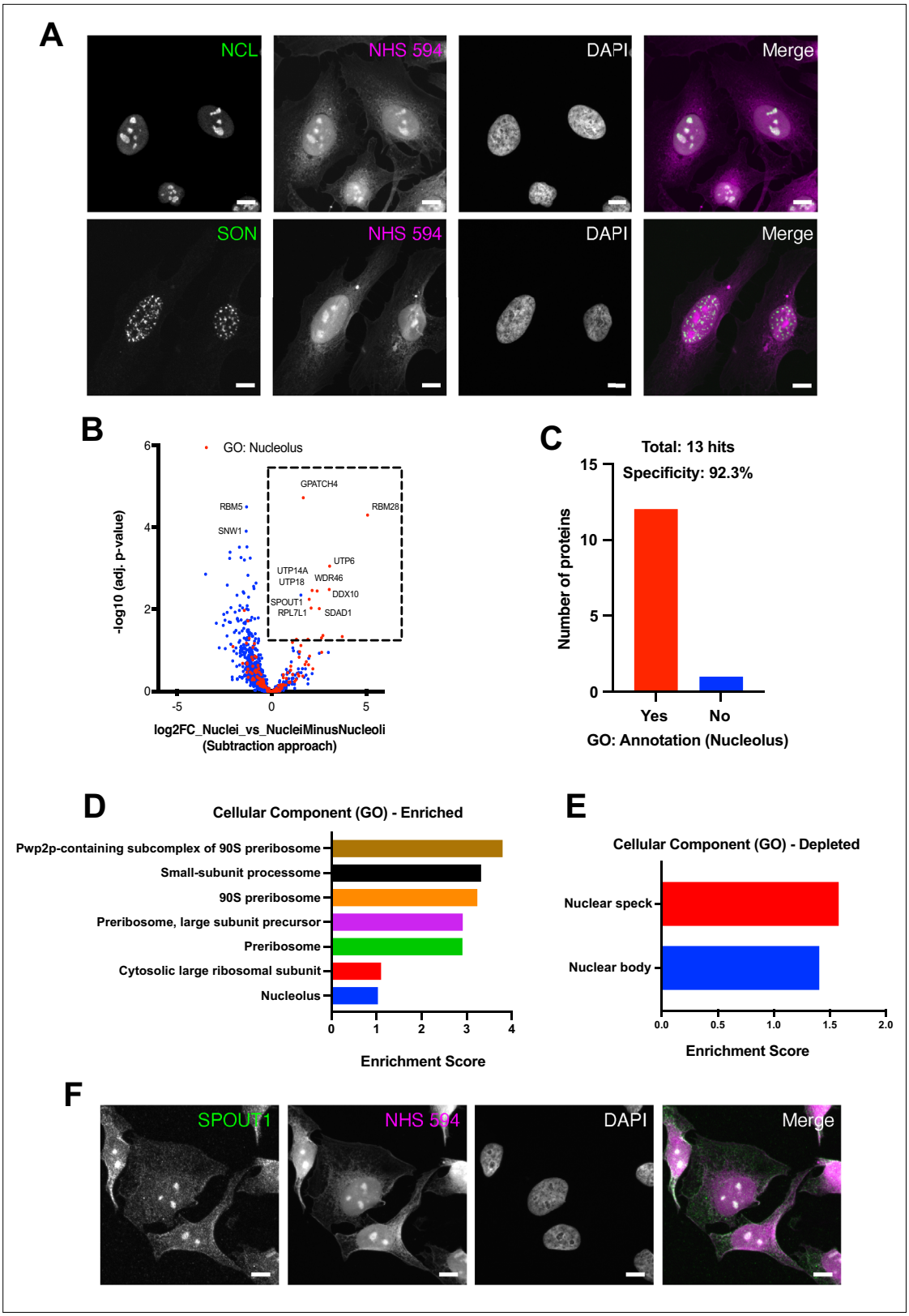


Figure 4. Application of SPEx (*Subcellular spatial Proteomics coupled to Expansion*) to nucleoli. (**A**) HeLa cells immunostained for NCL (nucleolar marker) or SON (nuclear speckle marker) and stained with DAPI and NHS 594. DAPI is omitted from the merged image for clarity. Scale bar, 10 µm. (**B**) Volcano plot of pairwise proteomic comparison between Nuclei and NucleiMinusNucleoli samples. The dotted square indicates proteins significantly enriched in nuclei (adjusted $p<0.05$, $\log_2 FC > 0$). Red dots represent proteins annotated to localize to the nucleolus according to Gene Ontology (GO).

Figure 4 continued on next page

Figure 4 continued

(**C**) Number of proteins significantly enriched in (**B**) that are annotated as nucleolar (Yes) or not (No) according to GO. (**D**) Functional enrichment analysis of all quantified proteins shown in (**B**) for cellular components using GO via STRING (https://string-db.org/). The seven most enriched significant terms (ranked by enrichment score) are shown. All significant terms (FDR <1%) are listed in ***Supplementary file 1K***. (**E**) Same analysis as in (**D**), showing the two significantly depleted GO terms. (**F**) HeLa cells immunostained for SPOUT1 and stained with DAPI and NHS 594. DAPI is omitted from the merged image for clarity. Scale bar, 10 µm.

The online version of this article includes the following figure supplement(s) for figure 4:

Figure supplement 1. Standard approach applied to the nucleoli and comparison of SPEx to SubCellBarCode.

in the nucleoplasm and the nucleoli, while their concentration could be still higher in the nucleoli. Moreover, the volume of the nucleus is much bigger than the combined volume of the nucleoli, which we excised, making quantitative comparison more challenging. To circumvent these problems, we applied the subtraction method to detect which proteins are reduced in the NucleiMinusNucleoli samples compared to the Nuclei samples. Using this method, we increased the specificity from 10.8 to 92.3%, at the expense of the number of specific hits (***Figure 4B***). Still, from the 13 significantly enriched proteins all but one, SPOUT1, were annotated by GO to be nucleolar (***Figure 4C***). We have already identified SPOUT1 as a novel nuclear protein above (***Figure 3B***). Our nucleoli analysis suggested that SPOUT1 is actually a nucleolar protein that we could confirm by IF (***Figure 4F***). This is in line with a study showing that the SPOUT1 homolog in *Drosophila* (Ptch) is a methyltransferase that methylates the 28 S rRNA in the *Drosophila* nucleolus and is essential for oogenesis (***Chen et al., 2024***). Moreover, functional enrichment analysis showed that proteins associated with the 90S pre-ribosome, which are specifically localized in the nucleolus, were highly enriched (***Figure 4D*** and ***Supplementary file 1K***). Thus, despite this high stringency, we were still able to identify a novel component of the nucleolus. It is worthwhile noting that while the subtraction method strongly reduced the number of potential false positives, the most significantly enriched proteins were also found by the standard method in which we compared Nucleoli to NucleiMinusNucleoli (***Figure 4B***, ***Figure 4—figure supplement 1A***), indicating that nucleoli proteins were also enriched in the excised nucleoli fraction. Moreover, the standard method might at times be more useful as a discovery tool. Nevertheless, we successfully identified proteins of the membraneless nucleolus using expanded in situ laser-dissected samples.

SPEx identifies nuclear speckle proteins absent from nucleoli

The nucleolus is not the only membraneless organelle in the nucleus. Like nucleoli, those other organelles, such as nuclear speckles, have a high local concentration of their protein components, but these proteins are likewise present in the nucleoplasm, and both pools are constantly exchanging. However, exchange between constituents of nucleoli with constituents of other nuclear membraneless organelles is expected to be limited. As a further test for specificity, we asked whether we could detect components of the other nuclear membraneless organelles in the fraction that is depleted or absent from nucleoli. In both, the standard and the subtraction method, RBM5 and SNW1 were very significantly depleted from the nucleoli fraction (***Figure 4B***, ***Figure 4—figure supplement 1A***). RBM5 is a component of the spliceosome A complex and SNW1 a component of the minor spliceosome. The spliceosome has been shown to be located in nuclear speckles (***Bhat et al., 2024***) and, according to Protein Atlas (***Figure 4—figure supplement 1D and E***; ***Thul et al., 2017***), RBM5 and SNW1 are indeed located in nuclear speckles and absent from the nucleolus. Moreover, functional enrichment analysis revealed that nuclear speckle and nuclear body proteins were significantly depleted from our nucleolar fraction (***Figure 4E*** and ***Supplementary file 1K***). Therefore, also for the nucleolus, we were able to determine proteins that were specifically depleted/absent from nucleoli in an environment, which is guided by protein diffusion.

SPEx compared to other spatial proteomics methods applied to the nucleolus

To date, only a few subcellular proteome studies assigned nucleolar locations to proteins, because membraneless organelles are notoriously difficult to purify (***Orre et al., 2019***; ***Supplementary file 1H***). By contrast, SPEx allows isolation and collection of organelles directly from cells and is therefore ideally suited for the enrichment and analysis of membraneless organelles. This is nicely demonstrated

by the higher specificity for nucleolar proteins obtained by SPEx (>90%) compared to classical density gradient centrifugation with only around 50% (***Orre et al., 2019***; ***Figure 4—figure supplement 1F and G***).

Taken together, SPEx not only allowed us to detect nucleolar proteins with very high specificity but also enables us to identify an unannotated nucleolar protein. Moreover, compared to other available methods, SPEx demonstrated a higher specificity in assigning proteins to a membraneless organelle, such as the nucleolus.

Golgi proteins are identified with high specificity using SPEx

Finally, we used SPEx to determine the proteome of the Golgi. The Golgi is a central sorting station for proteins and lipids and which is responsible for post-translational modifications such as glycosylation, sphingolipid synthesis, and sulfation. It is a highly dynamic structure, and transport through the Golgi and the dynamics of Golgi cisternae are still a matter of debate. To address these issues, it would be desirable to have a method, which could capture the Golgi in different states. Recently developed immunoprecipitation methods have tackled this challenge (***Fasimoye et al., 2023***); however, because of a few time-consuming purification steps, important transient molecular interactions might still be lost. SPEx, on the other hand, allows direct isolation of organelles from fixed cells with preserved molecular composition and should therefore be well suited for the analysis of this dynamic organelle.

To test this exciting possibility, we excised 35 Golgis from expanded and dried samples and performed LC-MS. First, we determined which percentage of the total protein mass in these samples is contributed by proteins GO annotated with Golgi or extracellular localization. The later class most likely represents cargo traveling through the Golgi. We found that 84.7% of the total protein mass is contributed by proteins belonging to one or both of those classes, indicating very good purity of the sample (***Figure 5—figure supplement 1A***). Next, we compared these Golgi samples to the corresponding cells without Golgi (CellsMinusGolgi; ***Figure 5A***). We identified 356 significantly enriched proteins in the Golgi samples, 288 (80.9%) were GO annotated with Golgi or extracellular localization (***Figure 5B***). Among the enriched proteins were many proteins related to glycosylation such as GALNT1, 2, and 7 (***Figure 5A***). We also detected several Golgins (GOLGA2-4); GOLGA2 (GM130) was our Golgi marker. Moreover, numerous trafficking-related Golgi proteins such as the SNARE receptor GOSR1, the COG tethering proteins, and the coatomer complex, which is the coat of COPI vesicles, were highly enriched in the Golgi fraction. The method was sensitive enough to also detect the Golgi Rab, Rab6A (***Figure 5A***). In contrast, endosomal proteins such as SNX2, CHMP4A and B, or EHD2 were depleted, as well as the components of the adaptor complex for clathrin-mediated endocytosis such as AP2A2 or the plasma membrane exocyst tether EXOC8 (***Figure 5A***). Interestingly, we also observed depletion of the ARP2/3 complex from the Golgi fraction. Notably, the comparison of WholeCells to CellsMinusGolgi revealed also Golgi-resident proteins (***Figure 5—figure supplement 1B***), but with a somewhat lower specificity (***Figure 5—figure supplement 1C***). The trend of the analysis is similar to what we observed for the analysis of the nucleus (WholeCells vs CellsMinusNucleus). Functional enrichment analysis confirmed the high specificity of Golgi proteins in our SPEx results. The most enriched cellular components were all associated with the Golgi (***Figure 5C*** and ***Supplementary file 1L***), whereas the most depleted protein groups were all assigned to the nucleus (***Figure 5D***). This result may not be very surprising because the nucleus has the highest protein content, and there is essentially no overlap with Golgi proteins.

Our analysis also identified proteins that were not annotated previously to be Golgi localized. We selected again one candidate, KIAA2013, for confirmation (***Figure 5A***) and determined the subcellular localization using IF (***Figure 5E***). Indeed, KIAA2013 was Golgi localized and, thus, again we were able to assign a new location to a protein. KIAA2013 remains very poorly characterized, but based on sequence analysis, the protein contains a short C-terminal cytoplasmic tail, a single transmembrane domain, and a large, potentially extracellular, N-terminal domain (***Bateman et al., 2025***). While our SPEx and IF data suggests that the bulk of KIAA2013 is retained at the Golgi, the additional cytoplasmic puncta raise the possibility that a fraction of KIAA2013 is trafficked beyond the Golgi, potentially to the plasma membrane or to endosomal compartments.

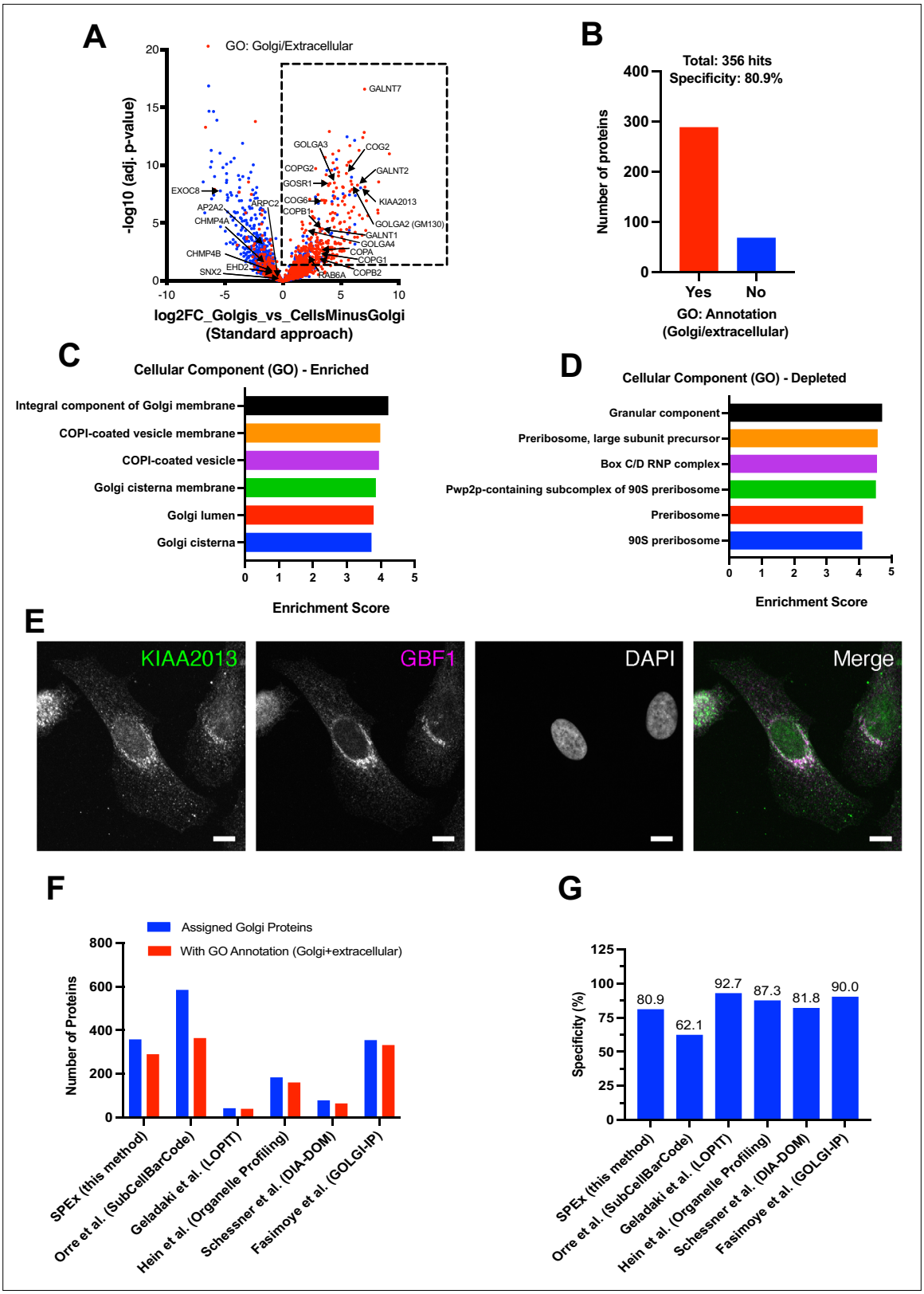


Figure 5. Application of SPEx (*Subcellular spatial Proteomics coupled to Expansion*) to the Golgi. (**A**) Volcano plot of pairwise proteomic comparison between Golgis and CellsMinusGolgi. The dotted square indicates proteins significantly enriched (adjusted $p<0.05$, $log_2FC >0$) in the Golgi. Red dots represent proteins annotated to localize to the Golgi and/or to be extracellular according to Gene Ontology (GO). (**B**) Number of proteins significantly enriched in the Golgi in (**A**) that are annotated as Golgi and/or extracellular (Yes) or not (No) according to GO. (**C**) Functional enrichment analysis of

Figure 5 continued on next page

Figure 5 continued

all quantified proteins shown in (**A**) for cellular components using GO via STRING (https://string-db.org/). The six most enriched terms (ranked by enrichment score, FDR <1%) are shown. All significant terms (FDR <1%) are listed in ***Supplementary file 1L***. (**D**) Same analysis as in (**C**), showing the six most depleted GO terms. (**E**) HeLa cells immunostained with antibodies for KIAA2013 and GBF1 (Golgi marker) and stained with DAPI. DAPI is not shown in the merged image for clarity. Scale bar, 10 µm. (**F**) Bar plot comparing the number of proteins assigned to the Golgi (blue) in our SPEx dataset (this study, **A**) with other published spatial proteomics datasets (***Fasimoye et al., 2023***; ***Geladaki et al., 2019***; ***Hein et al., 2025***; ***Orre et al., 2019***; ***Schessner et al., 2023***). Proteins overlapping with GO Golgi/extracellular annotations are shown in red. (**G**) Specificity of GO Golgi/extracellular annotation in the different proteomics datasets, determined from (**F**).

The online version of this article includes the following figure supplement(s) for figure 5:

Figure supplement 1. Subtraction approach applied to the Golgi and depiction of gelation chamber assembly and sample mounting.

SPEx compared to other spatial proteomics methods

Compared to previously published large-scale datasets (***Fasimoye et al., 2023***; ***Geladaki et al., 2019***; ***Hein et al., 2025***; ***Orre et al., 2019***; ***Schessner et al., 2023***; ***Supplementary file 1H,I,J,M and N***), SPEx achieved comparable results with a high proteome coverage (***Figure 5F***) and similar specificity (***Figure 5G***). Finally, we also compared SPEx to previously published methods combining ExM and spatial proteomics (***Dong et al., 2024***; ***Li et al., 2022***; ***Supplementary file 1O***). SPEx outperforms previously available methods with respect to spatial resolution. Thus, SPEx is the first method that allows LMD and LC-MS of structures significantly smaller than the nucleus, while maintaining good proteome coverage.

Discussion

Here, we report the development of SPEx as a method for in situ subcellular spatial proteomics at a single micrometer resolution. To achieve this, we combined ExM with laser dissection and LC-MS/MS. SPEx requires low sample input, is low cost, and adaptable to membrane-bounded and membraneless organelles. Depending on the size of the organelles, SPEx can be readily used for subcompartments of organelles.

Development of SPEx

To establish the protocol, we took advantage of the well-known TREx protocol, which allows up to 10x expansion without the need for any specialized equipment or procedures (***Damstra et al., 2022***). Drying the samples onto a PPS-membrane still maintained an about 7x linear expansion in x–y, resulting in almost 50x increase of surface area. This increase enlarges the subcellular regions to an extent that they can be easily excised by LMD. Depending on the size of the structure of interest, SPEx is also compatible with lower expansion factors, which can be fine-tuned by adding different amounts of the crosslinker (Bis) to the gelation solution. For example, we reached fourfold, sixfold, or tenfold expansion by using 0.1, 0.04, or 0.005% Bis, respectively. In this study, we focused on 10x expansion since it enables isolation of structures as small as nucleoli. In addition, we found that small differences in the amount of anchoring reagent (AcX) impacted the expansion factor of cells but not of the hydrogel. For this reason, we reduced anchoring from 0.1 mg/ml AcX to 0.05 mg/ml AcX compared to ***Damstra et al., 2022***. This reduction showed no negative effect on proteome coverage in LC-MS but improved expansion factor. In case the expansion factor is not consistent between sample and gel, we suggest titrating AcX concentrations between 0.01 mg/ml and 0.1 mg/ml to find optimal conditions. Moreover, the use of low amounts of glutaraldehyde (0.1%) during fixation is compatible with SPEx but might have a potential negative impact on the expansion factor due to increased crosslinking of the sample. Therefore, we would recommend the use of PFA only whenever possible. We also found that secondary antibodies and dyes in the red-emitting range (e.g. 594 nm) are likely to be better in the preservation of fluorescence throughout expansion and drying of the sample. We, therefore, usually visualized the most relevant structure in the red-emitting range. Testing other secondary antibodies and labeling techniques should provide more additional color options, which might be useful for double labeling experiments. Such double labeling will facilitate the determination of the proteome of membrane subcompartments such as membrane contact sites. Finally, SPEx might be compatible with other protease-free expansion workflows. However, we have not used other expansion methods, and compatibility would have to be assessed.

Another possible problem we considered is that lysine modifications during anchoring (or NHS labeling) might interfere with detection of the modified peptides during LC-MS and thus reduce coverage. We specifically searched for both modifications (NHS labeling and anchoring) in our LC-MS data but could not identify any such lysine modified peptides. Therefore, these modifications are either very sparse or not compatible with LC-MS analysis. To exclude the latter, we compared the ratio of peptides carrying a lysine at the last position to the peptides carrying an arginine at the last position. Since both amino acids are equally abundant in the human proteome and tryptic cleavage sites, lysine modifications will cause frequent miscleavage/prevent detection, and we would expect a strong bias toward peptides carrying an arginine at the last position. However, we did not observe such a bias (***Figure 2—figure supplement 1C***) and obtained very similar Lys/Arg ratios compared to other fixed, but not expanded, human samples, indicating that our expansion protocol has no detectable impact on lysine residues.

SPEx can be applied to a variety of subcellular targets

To demonstrate the general applicability of SPEx, we chose a diverse set of targets in this study: the nucleus, the nucleolus, and the Golgi. Those targets differ in size, shape, labeling method required for visualization (dyes and IF), and architecture (membrane-bound and membraneless organelles). Surprisingly, only a couple of dozens of organelles are required as sample input for LC-MS/MS for SPEx. These inputs were sufficient to obtain good coverage and high specificity. Importantly, we detected not only predicted or previously known components of these well-studied organelles. We also identified novel proteins residing in the nucleus, the nucleolus, and the Golgi with high specificity. Of note, membraneless organelles are inherently difficult to purify. SPEx overcomes this problem by eliminating the need for biochemical enrichment procedures. Moreover, SPEx compares favorably to other specialized enrichment procedures. We compared the coverage and specificity of SPEx to a number of currently available other spatial proteomics methods, based on either subcellular fractionation followed by proteome profiling (***Geladaki et al., 2019***; ***Orre et al., 2019***; ***Schessner et al., 2023***) or native immunoprecipitation proteomics of organelles (***Fasimoye et al., 2023***; ***Hein et al., 2025***). When applied to the nucleus or nucleoli, SPEx showed either better coverage or better specificity than currently available methods. When we employed SPEx to the Golgi, we were able to obtain coverage and specificity comparable to currently available methods including a specific Golgi-IP (***Fasimoye et al., 2023***). Another great advantage of SPEx is that it does not rely on transfection of fusion proteins, changes in the media, or other manipulations. Whatever method can be used to visualize the region or structure of interest is sufficient to perform SPEx. We used the same overall protocol for the sample preparation and the analysis of the nucleus, nucleoli, and Golgi, indicating that not much, if any, tinkering must be done to perform a successful SPEx experiment. Sampling of different structures from the same preparation (e.g. whole cells, nucleus, cells without nucleus, nucleoli, nuclei without nucleoli) abolishes the need for separate sample preparations for different targets and controls. Compared to other methods utilizing ExM to perform spatial proteomics (***Dong et al., 2024***; ***Li et al., 2022***), SPEx exhibits a significant improvement in spatial resolution, thus allowing the analysis of a large number of subcellular compartments.

Different analysis pipelines for SPEx data

Our data show that SPEx data can be analyzed efficiently in two different ways. The standard approach is to isolate structures of interest and compare their proteome to that of cells or subcellular compartments from which the structures were removed (control). The other, useful option is the subtraction approach, which is an indirect measure, but still very powerful. In this case, the structure of interest is cut out. The analysis, however, is performed on the cell/organelle from which the structure of interest has been excised and compared to the cell/organelle in which the structure is still present. Both approaches yield comparable results in our test cases. The standard approach is well-suited for most questions and approaches, and also for the discovery of transiently interacting or low-abundant proteins. Even though we employed median normalization to our proteomics data abundances, which controls for different sample amounts and eventually results in a comparison of protein concentration rather than pure protein abundances, it became clear that comparison of structures of very different sizes might be technically difficult and that in such cases, controls should be collected in a similar size range to the actually studied compartments. The subtraction method detects proteins that were lost

from one sample and is thereby highly specific and gives fewer false positives. This approach might be particularly useful when venturing into the unknown and markers of a compartment or domain need to be identified. Even though we obtain about sevenfold expansion of our dried samples, this magnification might not be sufficient to cut out and analyze tiny organellar subcompartments. In those cases, eliminating these structures from the sample might provide the specificity to identify key proteins of these structures.

SPEx performs best in a comparative approach

We have great resolution in the x–y direction (50x surface area increase); however, no resolution in z. We were, therefore, initially worried about potential contamination and false positive detection of proteins. To our delight, it turned out that this was not a big problem. Proteins present on an organelle will still be enriched in the sample, while the level of the cytoplasmic or plasma membrane proteins will remain at the same levels in the sample and the control, and hence these proteins are not enriched in the organellar fraction. Even though we may also cut out other organelles or pieces thereof, this will likewise happen in the control. For the nucleus and the Golgi, we also found that the vast majority of the protein mass in the sample is still contributed by proteins assigned to these respective compartments, indicating that even without comparing the samples to a control, the data would represent an albeit less clean proteome of the organelle. For much smaller compartments like the nucleolus, however, this comparative approach is likely essential. This is illustrated by the fact that, even though only a small part of the protein mass in our nucleoli samples was contributed by nucleolar proteins, comparison with a control allowed us to identify the same proteins as with the more stringent subtraction approach, although with lower specificity. Our data show that the lack of resolution in Z is a much lesser problem than initially anticipated.

Future directions

We think that SPEx holds great potential to answer spatial proteomics questions that were hard to tackle until to date. A great strength of SPEx is that the experimentalist specifically selects the (sub) compartments for the analysis, which is in marked difference to proximity labeling techniques. SPEx could, thus, be used to quantitatively determine the composition of fragmented vs fused mitochondria or between tubular and sheet endoplasmic reticulum in the same cell. We also foresee its use for detecting other organellar subcompartments. Moreover, compared to other spatial proteomics methods currently used, SPEx requires very little prior knowledge and no genetic manipulation of the studied system. Visualizing an organelle or compartment just by morphology would be sufficient for SPEx. Thus, even structures for which no antibodies are available could potentially be analyzed using SPEx. This, together with the fact that the TREx expansion method has been shown to be widely applicable to different cell types and tissue sections (***Damstra et al., 2022***), leads us to believe that SPEx could be a valuable tool to perform spatial proteomics on hard-to-transfect cells, tissues, and non-model organisms where genetic manipulation and/or antibody staining remains highly challenging.

Another potential application of SPEx lies in studying cell-to-cell heterogeneity because SPEx allows researchers not only to perform spatial proteomics on specific organelles but also to select the cells from which these organelles should be isolated. This would allow for comparative studies, where the proteome of specific organelles in morphologically different cells in the same dish (e.g. dividing vs non-dividing or responders vs non-responders in drug treatment) could be determined. This remains challenging with conventional methods, due to the generation of lysates from many cells prior to enrichment. Therefore, the analysis on the single-cell level remains difficult with these methods. Importantly, SPEx does allow these types of analyses.

It is conceivable that the SPEx approach could be used beyond the context of spatial proteomics. In the future, this approach could potentially be coupled to downstream lipidomics, allowing us to study the membrane composition of different organelles/domains in the cell. Possibly, the same workflow could also be used to perform RNA/DNA sequencing to determine the RNA content of condensates or the DNA content of specific nuclear regions. We also expect SPEx to work on tissue sections.

In summary, by combining ExM, LMD, and low input LC-MS, SPEx offers a novel approach to subcellular spatial proteomics. The low sample requirements and flexible nature of the SPEx method make it a useful approach to tackle spatial proteomics questions that were previously hard to investigate and required the development of highly specialized methods.

Materials and methods

Key resources table

Reagent type (species) or resource	Designation	Source or reference	Identifiers	Additional information
Antibody	NCL (Mouse Monoclonal)	Abcam	ab136649	Dilution (1:500)
Antibody	SON (Rabbit Polyclonal)	GeneTex	GTX123778	Dilution (1:5000)
Antibody	GOLGA2/GM130 (Rabbit Polyclonal)	Proteintech	11308–1-AP RRID:AB_2115327	Dilution (1:200)
Antibody	SPOUT1 (Rabbit Polyclonal)	Atlas Antibodies	HPA022990	Dilution (1:50)
Antibody	KIAA2013	Atlas antibodies	HPA060536	Dilution (1:10)
Antibody	GBF1 (Mouse Monoclonal)	BD Biosciences	612116 RRID:AB_399487	Dilution (1:200)
Antibody	C7ORF50	Atlas Antibodies	HPA052281	Dilution (1:65)
Antibody	Rabbit IgG Alexa Fluor 594 (Goat Polyclonal)	ThermoFisher	A-11012 RRID:AB_2534079	Dilution (1:200) for ExM, Dilution (1:500) for IF
Antibody	Mouse IgG Alexa Fluor 594 (Goat Polyclonal)	ThermoFisher	A-11005 RRID:AB_2534073	Dilution (1:500)
Antibody	Rabbit IgG Alexa Fluor 488 (Goat Polyclonal)	ThermoFisher	A-11008 RRID:AB_143165	Dilution (1:500)
Antibody	Mouse IgG Alexa Fluor 488 (Goat Polyclonal)	ThermoFisher	A-11001 RRID:AB_2534069	Dilution (1:500)
Cell line (*Homo sapiens*)	HeLa	ATCC	CCL-2 RRID:CVCL_0030	

Cell culture

HeLa cells were cultured at 37 °C and 5% CO_2 in growth media (Dulbecco's Modified Eagle Medium (DMEM) high-glucose medium [Sigma-Aldrich, D57969] with 10% FCS [Biowest, S1810], 1% penicillin–streptomycin [Sigma-Aldrich, P4333], 1 mM sodium pyruvate [Sigma-Aldrich, S8636], and 2 mM L-glutamine [Gibco, 25030–024]). Cells were regularly tested for mycoplasma using a Mycoplasma PCR detection kit (Applied Biological Materials, G238).

Fixation and immunofluorescence

50,000 HeLa cells were seeded on sterile 13-mm glass coverslips (VWR, 631–0150) in a 24-well plate (Sarstedt, 83.3922). Cells were incubated at 37 °C, 5% CO_2 O/N, washed once in PBS (Gibco, 20012–019) and fixed in 3% PFA (Sigma, F8775-500ML) in PBS for 10 min. Cells were washed 3 x in PBS and permeabilized with 0.1% Triton (Sigma, T8787-50ML) in PBS for 10 min. After permeabilization, cells were washed 3 x in PBS and incubated in blocking solution (1% BSA (Sigma-Aldrich, A9647-100G) in PBS) for 30 min. Coverslips were transferred to a wet chamber and incubated for 1 hr in primary antibody (for dilutions see key resources table) in blocking solution. Coverslips were washed 3x in PBS and incubated for 30 min in secondary antibody in blocking solution (for dilutions see key resources table). Cells were washed 3x in PBS. Cells were incubated with 1 µg/ml DAPI (Sigma-Aldrich, D9542-10MG) and 0.2 µg/ml NHS ATTO 594 (Sigma-Aldrich, 08741–1 MG-F) or NHS-ATTO 488 (Sigma, 41698–1 MG-F), where applicable, in PBS for 1 hr at 37 °C. After washing 3 x in PBS for 5 min, coverslips were mounted on Fluoromount-G (SouthernBiotech, 0100–01) and left to settle overnight in the dark. Unless mentioned otherwise, all steps were performed at room temperature (RT). Confocal images were acquired with Evident/Olympus Fluoview FV3000 laser scanning system equipped with solid-state lasers and a galvanometer scanner using a UPLSAPO 60×/1.30 objective with silicone oil (Evident/Olympus, Z81114) and FV31S-SW software. For all experiments, three biological replicates were performed.

SPEx workflow

Fixation and immunofluorescence for SPEx

Sterile 13-mm coverslips were prepared in a 24-well plate. Coverslips were coated by incubating them in coating solution (Fibronectin bovine plasma [Sigma-Aldrich, F1141-5MG] 1:200 in ddH_2O)

for 90 min at RT. The coating solution was aspirated, and the coverslips were air dried for 20 min and washed once in PBS. 20,000 HeLa cells were seeded in DMEM (low confluency [~30–40%] is crucial for optimal expansion) and incubated at 37 °C, 5% CO_2 O/N.

Cells were washed once in PBS and fixed for 10 min at 37 °C with pre-warmed fixation mix (4% PFA in PBS). Cells were washed 2x in PBS. If no IF was performed, cells were permeabilized for 10 min in 0.1% Triton in PBS and subsequently washed 3x in PBS (for non-IF samples proceed to 'TREx expansion). For IF, cells were blocked for 1 hr in blocking solution (3% BSA, 0.1% Triton in PBS) with gentle rocking. Next, cells were incubated with primary antibody (for dilutions see key resources table) in blocking solution for 3 hr with gentle rocking. Cells were washed 3×5 min in PBS with gentle rocking and incubated with secondary antibody (for dilutions see key resources table) in blocking buffer O/N at 4 °C with gentle rocking. Cells were washed 3×10 min in PBS with gentle rocking. Unless mentioned otherwise, all steps were performed at RT. Adapted from ***Damstra et al., 2022***.

TREx expansion

Prior to the expansion, gelation chambers and gelation solution were prepared as follows:

- Gelation chamber: Two holes of 3–4 mm diameter (spaced apart by ~3 mm) were punched into a microscopy-slide-sized piece of parafilm (Parafilm, PM-996) using a tissue puncher. The parafilm was then placed on a glass microscopy slide (Epredia, AG00008032E01MNZ20; paper side up) and adhered by repeatedly streaking over it with a second microscopy slide and removing the paper on the parafilm. Finally, streaking can be repeated without the paper attached, by putting a non-adhesive plastic foil over the parafilm and streaking over it again until the parafilm is perfectly adhered to the glass microscopy slide (***Figure 5—figure supplement 1D***, steps 1–4).
- Gelation solution: The base of the gelation solution (1.1 M sodium acrylate [Sigma, 408220-25 G], 2 M acrylamide [Sigma, A4058-100ML], 0.005% Bis [Sigma, M1533-25ML], 1 x PBS [Thermo Fischer, 70011044]) was mixed, aliquoted, and stored at –20 °C. Before gelation aliquots were thawed to RT (prevents incomplete sodium acrylate dissolution) and then placed on ice. Right before use, 0.15% TEMED (Sigma, S7653-250G) and 0.15% APS (Sigma, A3678-25g) were added, the solution was mixed thoroughly, and placed back on ice immediately.

Anchoring was performed by incubating cells for 1 hr in 0.05 mg/ml AcX (Invitrogen, A20770) in PBS. In case expansion of the gel and the sample are not equal, we suggest titrating AcX concentrations between 0.01 mg/ml and 0.1 mg/ml for optimal results. Cells were washed once in PBS. The coverslip was rinsed once in gelation solution, and 4 µl of gelation solution was added to each hole of the gelation chamber. The coverslip was placed on the gelation chamber with the cells facing down, and a second 18-mm square coverslip was put on top. Clamps were used to press down the coverslip during gelation to obtain thinner gels (***Figure 5—figure supplement 1D***, steps 5–8). The assembled gelation chamber was incubated for 1 hr at 37 °C. Gels were removed from the gelation chamber by adding a drop of PBS onto the gels before gently moving them from the microscopy slide/coverslip into 2 ml Eppendorf tubes using a spatula. Gels were rinsed twice in PBS. After piercing the cap of the Eppendorf tube with a syringe to prevent pressure build-up, non-proteolytic disruption was performed by incubating the gels in disruption buffer (5% SDS [Sigma, 436143-25G], 200 mM NaCl [Sigma, S7279-25G], 50 mM Tris pH 8 [Invitrogen, AM9855G]) O/N at 95 °C on a heating block. After disruption, gels were rinsed once in 0.4 M NaCl, followed by two 30 min washes in PBS with gentle rocking. Gels were stained with 20 µg/ml DAPI and 20 µg/ml NHS-ATTO 488 or NHS-ATTO 594 in PBS for 1 hr at 37 °C. After staining, gels were rinsed once in PBS and transferred to a container with large volumes of Milli-Q water. Gels were expanded for 2×30 minu in MilliQ-water with gentle rocking. The water was exchanged again, and gels were left to expand O/N with gentle rocking. Unless mentioned otherwise, all steps were performed at RT. Adapted from ***Damstra et al., 2022***. The hydrated gels were transferred into a 30-mm imaging dish (Ibidi, 81156) and imaged on a CSU-W1 spinning disk confocal (Evident/Olympus) mounted on a IX83 stand and equipped with diode lasers and Hamamatsu ORCA-Fusion sCMOS cameras. The images were acquired with a ×30 UPL S APO 1.05 NA silicon objective (Olympus) and cellSens Dimension software (Evident Scientific, version 4.3.1).

For the experiment shown in ***Figure 2—figure supplement 1A***: 0.1% Bis was used for gelation. Anchoring was performed overnight in 0.1 mg/ml AcX. Denaturation was performed for 3 hr at 80 °C.

These conditions were used to achieve 4x expansion. For any other experiments, the procedure described above was used to allow for 10x expansion.

Drying of gels onto membrane slides

Fully expanded gels were trimmed with a scalpel and placed on a steel frame slide with PPS-membrane (Leica, 11600294). Excess water was removed with a tissue paper. The slide was incubated at 37 °C for 3 hr to dry the gels. Membrane slides were stored at 4 °C in a desiccator in the dark until laser dissection.

Widefield images of dried samples (and corresponding non-expanded controls) were captured using the Zeiss Imager.M2 with an EC Plan-NEOFLUAR ×20/0.5 (air) objective and ZEISS ZEN 3.9 Software.

Laser microdissection

LMD was performed using a LMD7 (Leica Microsystems) equipped with an Ultra LMT350 stage, and a 12-bit K3M monochrome camera. A 349 nm diode-pumped solid-state laser was used for microdissection, and the samples were cut using a HC PL FLUOTAR 10x/0.30, a HC PL FLUOTAR L 40x/0.60 CORR XT, or a HC PL FLUOTAR L 63x/0.70 CORR XT (Leica, 11506505, 11506208, or 11506222, respectively) and samples were collected into a low bind 96-well plate (Eppendorf, EP0030129512). In the Leica LMD software (version 8.5), ROIs were outlined using the drawing tool and collected using the 'Middle Pulse' mode; objectives used and number of ROIs collected were adjusted for different sample types (***Supplementary file 1C***). Images pre- or post-cuts were done with either a HC PL FLUOTAR 10x/0.30, a HC PL FLUOTAR L 40x/0.60 CORR XT, or a HC PL FLUOTAR L 63x/0.70 CORR XT.

Sample preparation for LC-MS

To avoid sample loss, all buffers were added to the side of the well, followed by a quick spin. Whenever the sample was transferred, low-bind tips were used. After collection 7 µl of lysis buffer (100 mM tetraethyl ammonium bicarbonate [TEAB; Supelco, 18597], 0.02% n-dodecyl-ß-maltoside [DDM; Sigma, D4641], 10 mM tris(2-carboxyethyl)phosphine [Sigma-Aldrich, 626547], 15 mM 2-chloroacetamide [Sigma, C0267]), were added to the sample in the low bind 96-well plate. The sample was heated to 95 °C for 1 hr in a thermal cycler. After cooling of the sample to RT, 1 µl of digestion buffer (60% acetonitrile [ACN; EGT Chemie AG, RC-ACNMS-2.5L] and 100 mM TEAB) was added. Next, the sample was again heated to 75 °C for 30 min in a thermal cycler. After cooling the sample to RT, 2 µl of trypsin solution (10 ng/µl Trypsin [Promega, V5113], 50 mM TEAB, and 0.01% DDM) was added and the sample was incubated for 12 hr at 37 °C. The reaction was stopped by adding 1 µl of 5% trifluoracetic acid (TFA; Thermo Fisher, 28904), and the sample was dried in a speedvac (Labconco, centrivap).

Finally, the peptides were cleaned by solid phase extraction using EvoTip Pure stage tips (EVOSEP, EV2020). The dried samples were heated to 37 °C, resuspended in 10 µl resuspension buffer (0.1% TFA) using sonication for 5 min in a water bath. The sample was loaded onto EvoTips by centrifugation following the vendor's protocol. Peptides were eluted with 20 µl elution buffer (40% ACN, 0.1% formic acid [FA]) directly into a low bind 96-well plate, dried under vacuum, and stored at –20 °C until further use.

LC-MS analysis

Peptides were resuspended in 5 µl 0.1% FA, and the whole sample was used for LC-MS/MS analysis using a timsTOF Ultra 2 Mass Spectrometer (Bruker) fitted with a Vanquish Neo HPLC (Thermo Fisher Scientific). The column heater was set to 60 °C. Peptides were resolved using a RP-HPLC column (100 µm×30 cm) packed in-house with C18 resin (ReproSil Saphir 100 C18, 1.5 µm resin; Dr. Maisch GmbH) at a flow rate of 0.4 µl/min at 60 °C. A linear gradient of buffer B (80% ACN, 0.1% FA in water) ranging from 2 to 25% over 25 min and from 25 to 35% over 5 min was used for peptide separation. Buffer A was 0.1% FA in water. The mass spectrometer was operated in positive DIA-PASEF mode. MS spectra were acquired from 100 to 1700 m/z. For MS/MS, we used eight MS/MS ramps and 24 MS/MS windows covering a mass-to-charge ratio range of 400–1000 m/z. This resulted in 25 Th wide MS windows and an ion mobility range from 0.64 to 1.37 V -s/cm². The mass spectrometer was operated in normal sensitivity mode, expected cycle time was 0.95 s, and accumulation and ramp time was set to 100 ms. The following source settings were applied: 1600 V Capillary Voltage and 3 l/min Dry Gas

flow at 200 °C. The collision energy was linearly ramped between 20 eV at 0.6 V -s/cm² and 59 eV at 1.6 V -s/cm².

Data analysis

The acquired raw files were searched using SpectroNaut (Biognosys, Schlieren, Switzerland, v19.0, default settings) against a human database (consisting of 20,360 protein sequences downloaded from Uniprot on February 22, 2022) and 393 commonly observed contaminants using the following search criteria: full tryptic specificity was required (cleavage after lysine or arginine residues, unless followed by proline); three missed cleavages were allowed; carbamidomethylation (C) was set as fixed modification; oxidation (M), N-acetlyation (N-term) were applied as variable modifications. To ensure accurate and precise protein quantification, only raw files from samples analyzed completely and without any technical errors, like column clogging during LC-MS analysis, were considered. The raw quantitative data was further statically analyzed using ProteoFlux (v1.8.3, Mollet, D., and Schmidt, A. ProteoFlux [version 1.8.5; computer software]; https://doi.org/10.5281/zenodo.18640999) and Prism (v10.3.1, GraphPad). ProteoFlux is an open-source and reproducible workflow for quantitative proteomics data analysis. Prior to quantification, precursor intensities were filtered based on run-level posterior error probability and q-value thresholds (≤0.01), and very low-intensity signals (below a threshold of 2) were treated as left-censored measurements. Precursor-level intensities exported from Spectronaut were aggregated to peptide-level quantities and subsequently summarized to protein abundances using a simple summarization-based approach, followed by median-based sample normalization and statistical analysis using linear models with empirical Bayes moderation. Exploratory data analysis included PCA of normalized protein intensities after left-censored missing value imputation and visualization of protein identification overlaps between conditions using UpSet plots. For differential proteome analysis, the raw quantitative data was filtered as follows: only proteins quantified with at least two unique peptides and in at least three replicates in one condition per contrast were considered. Subcellular location annotations (GO, cellular compartment) for all human proteins were downloaded from https://www.uniprot.org (February 06, 2026; ***Supplementary file 1F***). Functional enrichment analysis was carried out using https://string-db.org/ (***Szklarczyk et al., 2025***) and the 'Proteins with Values/Ranks' search scheme with default settings. Here, all protein accession numbers with their corresponding ratios of a specific contrast were imported. Only enriched terms with a Benjamini-Hochberg corrected FDR rate of 0.01% were considered (***Supplementary file 1GK and L***). The specificity of a specific contrast was determined by dividing the number significant protein hits (ratio >0, adjusted p-value <0.05) with correct subcellular GO annotation to all significant hits. Along these lines, the specificity of published methods was determined in the same way, using the list of all proteins assigned to the corresponding subcellular location as input. Intensity-Based Absolute Quantification values were obtained directly from SpectroNaut to calculate the total and GO annotated protein mass within the samples.

Acknowledgements

This work was a collaboration between the Spang Lab, the Imaging Core Facility and the Proteomics Core Facility (all Biozentrum, Basel). The authors thank Dariush Mollet for his valuable assistance with data analysis, preparation of figures, and contributions to the methods section. We also thank the Hondele lab (Biozentrum, Basel) for providing antibodies against NCL and SON and the Spiess lab (former Biozentrum, Basel) for sharing the HeLa CCL2 cell line. Finally, we thank Paul Guichard and Virginie Hamel's lab (Université de Genève) and the FAME facility (FMI, Basel), especially Sabine Reither for productive discussions on expansion protocol optimization. This work was supported by the University of Basel and the Swiss National Science Foundation (310030_197779, 310030_219513, 320030–231859) to A Spang.

Additional information

Funding

Funder	Grant reference number	Author
Universität Basel		Curdin A Franziscus Alexia Ferrand Oliver Biehlmaier Alexander Schmidt Anne Spang
Schweizerischer Nationalfonds zur Förderung der Wissenschaftlichen Forschung	310030_197779	Anne Spang
Schweizerischer Nationalfonds zur Förderung der Wissenschaftlichen Forschung	310030_219513	Anne Spang
Schweizerischer Nationalfonds zur Förderung der Wissenschaftlichen Forschung	320030-231859	Anne Spang

The funders had no role in study design, data collection and interpretation, or the decision to submit the work for publication.

Author contributions

Curdin A Franziscus, Conceptualization, Data curation, Formal analysis, Validation, Investigation, Visualization, Methodology, Writing – original draft, Writing – review and editing; Alexia Ferrand, Conceptualization, Formal analysis, Investigation, Visualization, Methodology, Writing – review and editing; Oliver Biehlmaier, Conceptualization, Resources, Supervision, Writing – review and editing; Alexander Schmidt, Conceptualization, Data curation, Software, Formal analysis, Validation, Investigation, Visualization, Methodology, Writing – original draft, Writing – review and editing; Anne Spang, Conceptualization, Resources, Data curation, Formal analysis, Supervision, Methodology, Writing – original draft, Project administration, Writing – review and editing

Author ORCIDs

Curdin A Franziscus https://orcid.org/0009-0008-4248-8848
Alexia Ferrand https://orcid.org/0000-0001-7292-1325
Oliver Biehlmaier https://orcid.org/0000-0003-0825-8500
Alexander Schmidt https://orcid.org/0000-0002-3149-2381
Anne Spang https://orcid.org/0000-0002-2387-6203

Peer review material

Version of Record:
Reviewer #1 (Public review): https://doi.org/10.7554/eLife.111393.3.sa1
Reviewer #2 (Public review): https://doi.org/10.7554/eLife.111393.3.sa2
Reviewer #3 (Public review): https://doi.org/10.7554/eLife.111393.3.sa3
Author response https://doi.org/10.7554/eLife.111393.3.sa4

Reviewed preprint v2
Reviewer #1 (Public review): https://doi.org/10.7554/eLife.111393.2.sa3
Reviewer #2 (Public review): https://doi.org/10.7554/eLife.111393.2.sa2
Reviewer #3 (Public review): https://doi.org/10.7554/eLife.111393.2.sa1
Author response: https://doi.org/10.7554/eLife.111393.2.sa0
eLife Assessment https://doi.org/10.7554/eLife.111393.2.sa4

Reviewed preprint v1
Reviewer #1 (Public review): https://doi.org/10.7554/eLife.111393.1.sa2
Reviewer #2 (Public review): https://doi.org/10.7554/eLife.111393.1.sa1
Reviewer #3 (Public review): https://doi.org/10.7554/eLife.111393.1.sa0
Author Response: https://doi.org/10.7554/eLife.111393.1.sa4
eLife Assessment https://doi.org/10.7554/eLife.111393.1.sa3

Additional files

Supplementary files

Supplementary file 1. Supplementary Tables. **Table A:** Experimental design of SPEx input test samples. **Table B:** Protein identifications obtained for SPEx input test samples. Table C: Number of samples collected and objectives used for laser microdissections with the LMD7 system. **Table D:** Experimental design of SPEx organelle analysis samples. **Table E:** Protein identifications for SPEx organelle analysis samples. **Table F:** GO terms, keywords, and cellular locations of all human proteins downloaded from UniProt (06/02/2026). **Table G:** Functional enrichment analysis of Nuclei_vs_CellsminusNuclei for Cellular Components (GO) using https://string-db.org/. **Table H:** Proteins with assigned subcellular locations according to ***Orre et al., 2019***, SubCellBarCode, Table S3 ("MCF7" sheet). Table I: Proteins with assigned subcellular locations according to ***Geladaki et al., 2019***, LOPIT, Supplementary Data 2. **Table J:** Proteins with assigned subcellular locations according to ***Hein et al., 2025***, Table S5 ("aggregate_annotation_literature" sheet). **Table K:** Functional enrichment analysis of Nuclei_vs_NucleiminusNucleoli for Cellular Components (GO) using https://string-db.org/. Table L: Functional enrichment analysis of Golgi_vs_CellsminusGolgi for Cellular Components (GO) using https://string-db.org/. **Table M:** Proteins with assigned subcellular locations according to ***Schessner et al., 2023***, DIA-DOMs, Supplementary Data 1. Only proteins with a location confidence of medium or higher were considered for the comparison. **Table N:** Proteins with assigned subcellular locations according to ***Fasimoye et al., 2023***, Golgi-IP, Supporting Information, Dataset S01 ("Golgi enriched" sheet). **Table O:** Comparison of SPEx to other methods utilizing ExM for spatial proteomics.

MDAR checklist

Data availability

All data are included in the main text or supplementary. All mass spectrometry proteomics data associated with this manuscript have been deposited to the ProteomicsXchange consortium via MassIVE (https://massive.ucsd.edu) with the accession number MSV000101122/PXD075606.
The following datasets were generated: ***Franziscus et al., 2026***

References

Bateman A, Martin MJ, Orchard S, Magrane M, Adesina A, Ahmad S, Bowler-Barnett EH, Bye-A-Jee H, Carpentier D, Denny P, Fan J, Garmiri P, Gonzales L, Hussein A, Ignatchenko A, Insana G, Ishtiaq R, Joshi V, Jyothi D, Kandasaamy S, et al. 2025. UniProt: the universal protein knowledgebase in 2025. *Nucleic Acids Research* **53**:D609–D617. DOI: https://doi.org/10.1093/nar/gkae1010, PMID: 39552041

Bhat P, Chow A, Emert B, Ettlin O, Quinodoz SA, Strehle M, Takei Y, Burr A, Goronzy IN, Chen AW, Huang W, Ferrer JLM, Soehalim E, Goh ST, Chari T, Sullivan DK, Blanco MR, Guttman M. 2024. Genome organization around nuclear speckles drives mRNA splicing efficiency. *Nature* **629**:1165–1173. DOI: https://doi.org/10.1038/s41586-024-07429-6, PMID: 38720076

Brunner A-D, Thielert M, Vasilopoulou C, Ammar C, Coscia F, Mund A, Hoerning OB, Bache N, Apalategui A, Lubeck M, Richter S, Fischer DS, Raether O, Park MA, Meier F, Theis FJ, Mann M. 2022. Ultra-high sensitivity mass spectrometry quantifies single-cell proteome changes upon perturbation. *Molecular Systems Biology* **18**:e10798. DOI: https://doi.org/10.15252/msb.202110798, PMID: 35226415

Chang HJ, Cheung CHY, Chong WM, Lu HH. 2024. Microscoop: two photon-induced biotinylation of protein constituents with submicron specificity. Syncell.

Chen F, Tillberg PW, Boyden ES. 2015. Expansion microscopy. *Science* **347**:543–548. DOI: https://doi.org/10.1126/science.1260088

Chen YD, Chang CW, Cheung CHY, Chang HJ, Sie YD, Chung CW, Huang CK, Huang CC, Chong WM, Liu YP, Lin YC, Kai HJJ, Wang PJ, Liao JC. 2023. Microscopy-guided subcellular proteomic discovery by high-speed ultra-content photo-biotinylation. *bioRxiv*. DOI: https://doi.org/10.1101/2023.12.27.573388

Chen J, Bai Y, Huang Y, Cui M, Wang Y, Gu Z, Wu X, Li Y, Rong YS. 2024. The Ptch/SPOUT1 methyltransferase deposits an m^3U modification on 28*S* rRNA for normal ribosomal function in flies and humans. *Science Advances* **10**:eadr1743. DOI: https://doi.org/10.1126/sciadv.adr1743, PMID: 39671501

Cho NH, Cheveralls KC, Brunner AD, Kim K, Michaelis AC, Raghavan P, Kobayashi H, Savy L, Li JY, Canaj H, Kim JYS, Stewart EM, Gnann C, McCarthy F, Cabrera JP, Brunetti RM, Chhun BB, Dingle G, Hein MY, Huang B, et al. 2022. OpenCell: Endogenous tagging for the cartography of human cellular organization. *Science* **375**:eabi6983. DOI: https://doi.org/10.1126/science.abi6983, PMID: 35271311

Damstra HGJ, Mohar B, Eddison M, Akhmanova A, Kapitein LC, Tillberg PW. 2022. Visualizing cellular and tissue ultrastructure using ten-fold robust expansion microscopy (TREx). *eLife* **11**:e73775. DOI: https://doi.org/10.7554/eLife.73775, PMID: 35179128

Domazet B, Maclennan GT, Lopez-Beltran A, Montironi R, Cheng L. 2008. Laser capture microdissection in the genomic and proteomic era: targeting the genetic basis of cancer. *International Journal of Clinical and Experimental Pathology* **1**:475–488 PMID: 18787684.

Dong Z, Jiang W, Wu C, Chen T, Chen J, Ding X, Zheng S, Piatkevich KD, Zhu Y, Guo T. 2024. Spatial proteomics of single cells and organelles on tissue slides using filter-aided expansion proteomics. *Nature Communications* **15**:9378. DOI: https://doi.org/10.1038/s41467-024-53683-7, PMID: 39477916

Fasimoye R, Dong W, Nirujogi RS, Rawat ES, Iguchi M, Nyame K, Phung TK, Bagnoli E, Prescott AR, Alessi DR, Abu-Remaileh M. 2023. Golgi-IP, a tool for multimodal analysis of Golgi molecular content. *PNAS* **120**:e2219953120. DOI: https://doi.org/10.1073/pnas.2219953120, PMID: 37155866

Franziscus CA, Ferrand A, Biehlmaier O, Schmidt A, Spang A. 2026. SPEx - Subcellular spatial Proteomics coupled to Expansion. *MassIVE*. http://massive.ucsd.edu/ProteoSAFe/dataset.jsp?task=661cefa3721e45c59477403b64f3f3b9

Gambarotto D, Zwettler FU, Le Guennec M, Schmidt-Cernohorska M, Fortun D, Borgers S, Heine J, Schloetel JG, Reuss M, Unser M, Boyden ES, Sauer M, Hamel V, Guichard P. 2019. Imaging cellular ultrastructures using expansion microscopy (U-ExM). *Nature Methods* **16**:71–74. DOI: https://doi.org/10.1038/s41592-018-0238-1, PMID: 30559430

Geladaki A, Kočevar Britovšek N, Breckels LM, Smith TS, Vennard OL, Mulvey CM, Crook OM, Gatto L, Lilley KS. 2019. Combining LOPIT with differential ultracentrifugation for high-resolution spatial proteomics. *Nature Communications* **10**:331. DOI: https://doi.org/10.1038/s41467-018-08191-w, PMID: 30659192

Guzman UH, Martinez-Val A, Ye Z, Damoc E, Arrey TN, Pashkova A, Renuse S, Denisov E, Petzoldt J, Peterson AC, Harking F, Østergaard O, Rydbirk R, Aznar S, Stewart H, Xuan Y, Hermanson D, Horning S, Hock C, Makarov A, et al. 2024. Ultra-fast label-free quantification and comprehensive proteome coverage with narrow-window data-independent acquisition. *Nature Biotechnology* **42**:1855–1866. DOI: https://doi.org/10.1038/s41587-023-02099-7, PMID: 38302753

Hein MY, Peng D, Todorova V, McCarthy F, Kim K, Liu C, Savy L, Januel C, Baltazar-Nunez R, Sekhar M, Vaid S, Bax S, Vangipuram M, Burgess J, Njoya L, Wang E, Ivanov IE, Byrum JR, Pradeep S, Gonzalez CG, et al. 2025. Global organelle profiling reveals subcellular localization and remodeling at proteome scale. *Cell* **188**:1137–1155. DOI: https://doi.org/10.1016/j.cell.2024.11.028, PMID: 39742809

Herrera JA, Mallikarjun V, Rosini S, Montero MA, Lawless C, Warwood S, O'Cualain R, Knight D, Schwartz MA, Swift J. 2020. Laser capture microdissection coupled mass spectrometry (LCM-MS) for spatially resolved analysis of formalin-fixed and stained human lung tissues. *Clinical Proteomics* **17**:24. DOI: https://doi.org/10.1186/s12014-020-09287-6, PMID: 32565759

Hondele M, Sachdev R, Heinrich S, Wang J, Vallotton P, Fontoura BMA, Weis K. 2019. DEAD-box ATPases are global regulators of phase-separated organelles. *Nature* **573**:144–148. DOI: https://doi.org/10.1038/s41586-019-1502-y, PMID: 31435012

Hundley FV, Gonzalez-Lozano MA, Gottschalk LM, Cook ANK, Zhang J, Paulo JA, Harper JW. 2024. Endo-IP and lyso-IP toolkit for endolysosomal profiling of human-induced neurons. *PNAS* **121**:e2419079121. DOI: https://doi.org/10.1073/pnas.2419079121, PMID: 39636867

Krautbauer S, Neumeier M, Haberl EM, Pohl R, Feder S, Eisinger K, Rein-Fischboeck L, Buechler C. 2019. The utrophin-beta 2 syntrophin complex regulates adipocyte lipid droplet size independent of adipogenesis. *Molecular and Cellular Biochemistry* **452**:29–39. DOI: https://doi.org/10.1007/s11010-018-3409-6, PMID: 30014220

Le Large TYS, Mantini G, Meijer LL, Pham TV, Funel N, van Grieken NCT, Kok B, Knol J, van Laarhoven HWM, Piersma SR, Jimenez CR, Kazemier G, Giovannetti E, Bijlsma MF. 2020. Microdissected pancreatic cancer proteomes reveal tumor heterogeneity and therapeutic targets. *JCI Insight* **5**:e138290. DOI: https://doi.org/10.1172/jci.insight.138290, PMID: 32634123

Li L, Sun C, Sun Y, Dong Z, Wu R, Sun X, Zhang H, Jiang W, Zhou Y, Cen X, Cai S, Xia H, Zhu Y, Guo T, Piatkevich KD. 2022. Spatially resolved proteomics via tissue expansion. *Nature Communications* **13**:7242. DOI: https://doi.org/10.1038/s41467-022-34824-2, PMID: 36450705

Liffner B, Silva T, Vega-Rodriguez J, Absalon S. 2024. Mosquito tissue ultrastructure-expansion microscopy (MoTissU-ExM) enables ultrastructural and anatomical analysis of malaria parasites and their mosquito. *BMC Methods* **1**:13. DOI: https://doi.org/10.1186/s44330-024-00013-4, PMID: 41426079

Lundberg E, Borner GHH. 2019. Spatial proteomics: a powerful discovery tool for cell biology. *Nature Reviews. Molecular Cell Biology* **20**:285–302. DOI: https://doi.org/10.1038/s41580-018-0094-y, PMID: 30659282

Makhmut A, Dragomir MP, Fritzsche S, Moebs M, Schmitt WD, Taube ET, Coscia F. 2026. Spatial proteomics of ovarian cancer precursors delineates early disease changes and drug targets. *Molecular Systems Biology* **22**:7–41. DOI: https://doi.org/10.1038/s44320-025-00168-4, PMID: 41233595

Nirschl JJ, Magiera MM, Lazarus JE, Janke C, Holzbaur ELF. 2016. α-tubulin tyrosination and CLIP-170 phosphorylation regulate the initiation of dynein-driven transport in neurons. *Cell Reports* **14**:2637–2652. DOI: https://doi.org/10.1016/j.celrep.2016.02.046, PMID: 26972003

Orre LM, Vesterlund M, Pan Y, Arslan T, Zhu Y, Fernandez Woodbridge A, Frings O, Fredlund E, Lehtiö J. 2019. SubCellBarCode: proteome-wide mapping of protein localization and relocalization. *Molecular Cell* **73**:166–182.. DOI: https://doi.org/10.1016/j.molcel.2018.11.035, PMID: 30609389

Perez F, Diamantopoulos GS, Stalder R, Kreis TE. 1999. CLIP-170 highlights growing microtubule ends in vivo. *Cell* **96**:517–527. DOI: https://doi.org/10.1016/s0092-8674(00)80656-x, PMID: 10052454

Rosenberger FA, Thielert M, Strauss MT, Schweizer L, Ammar C, Mädler SC, Metousis A, Skowronek P, Wahle M, Madden K, Gote-Schniering J, Semenova A, Schiller HB, Rodriguez E, Nordmann TM, Mund A, Mann M. 2023. Spatial single-cell mass spectrometry defines zonation of the hepatocyte proteome. *Nature Methods* **20**:1530–1536. DOI: https://doi.org/10.1038/s41592-023-02007-6, PMID: 37783884

Rosenberger FA, Mädler SC, Thorhauge KH, Steigerwald S, Fromme M, Lebedev M, Weiss CAM, Oeller M, Wahle M, Metousis A, Zwiebel M, Schmacke NA, Detlefsen S, Boor P, Fabián O, Fraňková S, Krag A, Strnad P, Mann M. 2025. Deep Visual Proteomics maps proteotoxicity in a genetic liver disease. *Nature* **642**:484–491. DOI: https://doi.org/10.1038/s41586-025-08885-4, PMID: 40240610

Roux KJ, Kim DI, Raida M, Burke B. 2012. A promiscuous biotin ligase fusion protein identifies proximal and interacting proteins in mammalian cells. *The Journal of Cell Biology* **196**:801–810. DOI: https://doi.org/10.1083/jcb.201112098, PMID: 22412018

Schessner JP, Albrecht V, Davies AK, Sinitcyn P, Borner GHH. 2023. Deep and fast label-free dynamic organellar mapping. *Nature Communications* **14**:5252. DOI: https://doi.org/10.1038/s41467-023-41000-7, PMID: 37644046

Sheard TMD, Shakespeare TB, Seehra RS, Spencer ME, Suen KM, Jayasinghe I. 2023. Differential labelling of human sub-cellular compartments with fluorescent dye esters and expansion microscopy. *Nanoscale* **15**:18489–18499. DOI: https://doi.org/10.1039/d3nr01129a, PMID: 37942554

Su H, Kodiha M, Lee S, Stochaj U. 2013. Identification of novel markers that demarcate the nucleolus during severe stress and chemotherapeutic treatment. *PLOS ONE* **8**:e80237. DOI: https://doi.org/10.1371/journal.pone.0080237, PMID: 24223222

Sun J, Yang M, Li Q, Liang J, Feng H, Gao L, Wang Y, Liu H, Guo C, Tang TS. 2026. mTOR-NAA10-C7orf50 axis senses nutritional status to coordinate ribosome biogenesis and autophagy. *Science Advances* **12**:eadz3835. DOI: https://doi.org/10.1126/sciadv.adz3835, PMID: 42139339

Szklarczyk D, Nastou K, Koutrouli M, Kirsch R, Mehryary F, Hachilif R, Hu D, Peluso ME, Huang Q, Fang T, Doncheva NT, Pyysalo S, Bork P, Jensen LJ, von Mering C. 2025. The STRING database in 2025: protein networks with directionality of regulation. *Nucleic Acids Research* **53**:D730–D737. DOI: https://doi.org/10.1093/nar/gkae1113, PMID: 39558183

The Human Protein Atlas. 2026. The human protein atlas. Version: 26.0. . https://www.proteinatlas.org/

Thul PJ, Åkesson L, Wiking M, Mahdessian D, Geladaki A, Ait Blal H, Alm T, Asplund A, Björk L, Breckels LM, Bäckström A, Danielsson F, Fagerberg L, Fall J, Gatto L, Gnann C, Hober S, Hjelmare M, Johansson F, Lee S, et al. 2017. A subcellular map of the human proteome. *Science* **356**:eaal3321. DOI: https://doi.org/10.1126/science.aal3321, PMID: 28495876

Tillberg PW, Chen F, Piatkevich KD, Zhao Y, Yu CC, English BP, Gao L, Martorell A, Suk HJ, Yoshida F, DeGennaro EM, Roossien DH, Gong G, Seneviratne U, Tannenbaum SR, Desimone R, Cai D, Boyden ES. 2016. Protein-retention expansion microscopy of cells and tissues labeled using standard fluorescent proteins and antibodies. *Nature Biotechnology* **34**:987–992. DOI: https://doi.org/10.1038/nbt.3625, PMID: 27376584

Walavalkar K, Gupta S, Kresoja-Rakic J, Raingeval M, Mungo C, Rubin P, Santoro R. 2025. Single-cell dynamics of genome-nucleolus interactions captured by nucleolar laser microdissection (NoLMseq). *Nature Communications* **16**:11417. DOI: https://doi.org/10.1038/s41467-025-66294-7, PMID: 41408051

Wen G, Leen V, Rohand T, Sauer M, Hofkens J. 2023. Current progress in expansion microscopy: chemical strategies and applications. *Chemical Reviews* **123**:3299–3323. DOI: https://doi.org/10.1021/acs.chemrev.2c00711, PMID: 36881995